Design and Analysis of a Biped Leg to Survive High-Impact Falls

Roberto O. Shu

CMU-RI-TR-16-21

Submitted in partial fulfillment of the requirements
for the degree of Master of Science in Robotics.

The Robotics Institute
Carnegie Mellon University
Pittsburgh, PA 15213

May 2016

Thesis Committee:
Koushil Sreenath, Chair
Hartmut Geyer
Nitish Thatte

Abstract

Humans have a remarkable agility and can perform explosive and dynamic motions such as walking, running, jumping and landing. This is in part due to the ability to handle large magnitude ground reaction forces (GRF) in conjunction with outstanding control capabilities of our body. On the other hand robotic bipedal systems have shown limited capabilities. Therefore, performing comparable levels of athleticism and robustness to perform explosive actions as humans, is still a challenge for bipedal systems.

In this thesis work we present our efforts to extend the capabilities of bipedal systems to include the ability to perform high impact drop jumps. We define drops jumps as the action starting at a given height above ground, followed by a free-fall phase, and finished by impacting the ground feet first. As a proof of concept we focused on the development of a novel mechanical design of a single robotic leg. Our proposed mechanical design minimizes the overall mass and inertia of the leg, augment actuators' power and implement an impact attenuation system based on a fiberglass leaf spring and a semi-active magneto-rheological damper.

A 3D CAD model of the final mechanical design was built, which was further used to develop a comprehensive simulation model of the leg in Matlab's Simscape environment. We draw inspiration from biomechanics and implement an impedance control to perform simulated drop jump experiments. Optimization techniques are used to find optimal gains for the impedance control. Simulation results show the importances and usefulness of having a physical damping mechanism on the leg to perform safe and controllable drop jumps from heights greater than 3 meters.

The results of this thesis are intended to be used in the development of a bipedal robot that is capable of dynamic walking, running, and other high impact motions such as drop jumping.

In addition to the work on legged robot, we also report preliminary results on the implementation of a nano aerial vehicle testbed for advance control algorithms. The proposed testbed was developed around the open-source Crazyflie Nano Quadcopter by Bitcraze. A motion capture arena is used to track the global position of the quadcopter. The a position trajectory tracking controller was implemented. Trajectory tracking experiments demonstrate the current capability of the proposed control framework to track trajectories within 10cm.

Thesis supervisor: Koushil Sreenath
Assistant Professor, Mechanical Engineering

Acknowledgments

I would like to especially thank my advisor Professor Koushil Sreenath. I am gratefully for the opportunity to work under his guidance and the continuous support throughout the development of this work.

Also, I thank Project Scientist Ben Brown for sharing his vast experience in mechanical design with me, and aid me on the leg design proposed in this work. I want to acknowledge the members of my thesis committee Professor Hartmut Geyer and PhD Student Nitish Thatte for their time reviewing and evaluating this work.

I would like to express gratitude to many others that assisted me during my work. Many thanks to PhD student Avinash Siravuru with whom I shared countless working and brainstorming sessions. I also want to thank PhD student Guofan Wu who taught me a vast amount of tools needed to work with quad rotors.

Finally, this work was supported in part by the scholarship program ”Universities of Excellence” from the Secretary of Higher Education, Science, Technology and Innovation (SENESCYT) of the Republic of Ecuador.

Contents

List of Figures

List of Tables

Part 1

Design and Analysis of a Biped Leg to Survive High-Impact Falls

Chapter 1

Introduction

1.1 Motivation

Humans have a remarkable agility and can perform explosive and dynamic motions such as running, jumping and landing from large heights. This is in part due to the ability to handle large magnitude ground reaction forces (GRF) in conjunction with outstanding control capabilities of our body. Through training this capabilities can be can enhanced [8] to perform high agility explosive maneuvers. For example a basketball player, during the landing after a layup jump shot may experience a GRF value up to 9 times its body mass without suffering an injury [9]. Bipedal robotic systems on the other hand have shown limited capabilities in terms of performing comparable levels of explosive behaviours as humans.

A wide variety of athletic movements, such as those performed in acrobatics or free-running (parkour), involve frequent transitions between airborne and ground-contact phases. Therefore, how to land to safely and efficiently break a fall is a fundamental skill to perform dynamic motions. Most humanoid robots developed so far are quite fragile and can not withstand large impacts. The impact from a fall can cause a legged robot to fail structurally (i.e. break a structural component) or mechanically (i.e. actuator overload). Further, they are primarily designed for walking or running not for jumping and landing.

We believe that before being able to deploy legged robots outside a constrained laboratory environment into hazardous, unconstructed, unexplored environments and be of aid to humans they have to be capable of smoothly performing dynamic motions. In this thesis work we present our efforts to extend the capabilities of bipedal systems to include the ability perform high impact drop jumps. We focus on the primary task of controllably and safely landing drop jumps from at least a second floor ($\approx$3m high). We propose a design for a new bipedal robotic leg and simple control strategies that; dissipates the kinetic energy accrued from the drop jump, protects the hardware from damage, and control the leg after impact.

1.2 Relevant Work

In the recent years there has been a significant increase in interest to improve the humanoid robotic systems capabilities to handle falls. This area of study gained significantly popularity

after the 2015 Darpa Robotic Challenge (DRC) Finals, where all teams experienced failures due to falls.

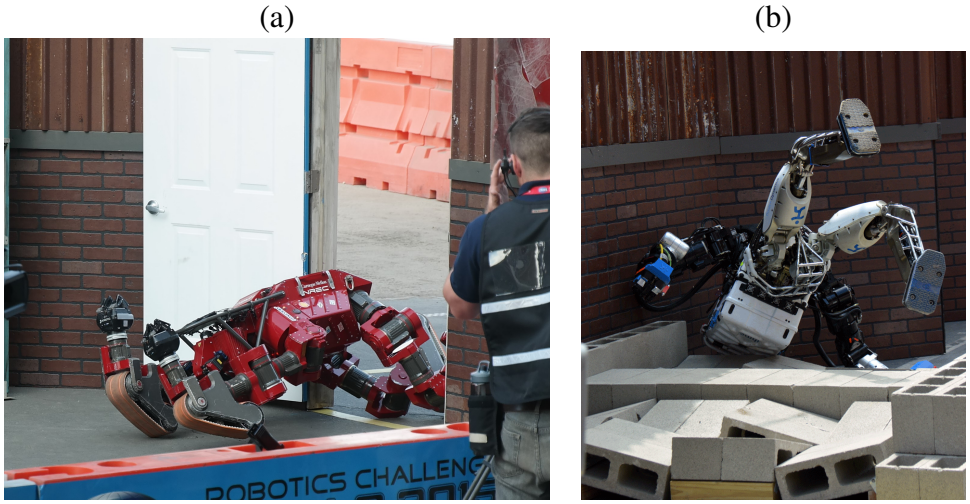

Figure 1.1: Images of fallen robots in Darpa Robotics Challenge (a) CMU-CHIMP and (b) IHMC Atlas robots

1.2.1 Human Strategies

In the field of biomechanics the landing phase of a jump has been widely studied [9, 10, 11]. Humans use several techniques to decrease the body's vertical momentum upon impact with the ground. Numerous studies have demonstrated that soft landings (low peak GRF) are generally characterized by greater amounts of flexion and energy absorbed by the knee and hip joints, while stiff (high peak GRF) landings exhibit high ankle and knee energy absorption with reductions in hip energy absorption [12, 13, 14]. In drops jumps from 20cm it was experimentally recorded that the total work done is distributed 24%, 54%, and 22% through the hip, knee and ankle joint respectively [14]. Evidently the knee joint muscles are absorbing most of the shock. With muscle fatigue there is an increase in ankle joint work and peak GRF [14]. Further suggesting the importance of the knee over the ankle joint for reducing the impact of drop jumps.

Attenuating the impact through knee flexion is referred as cushioning reflexion [11]. Due to the short duration of impact the lower body joint configuration at initial contact has a major influence on energy absorption during landing task [11, 12]. The human physiology allows for internal regulation of the joint and body compliance. Additionally, all the soft tissue in our bodies (e.g skin and muscles) are good at absorbing the impact shocks.

Humans also use more sophisticated techniques to attenuate the impact. An example of this are practitioners of Parkour (traceurs) who exploit human body capabilities. Traceurs mainly use two landing techniques to break falls; precision and roll landing [15]. Precision landing is categorized by a forefoot touchdown (no heel contact), bending of the knees to absorb impact, and the use of the arms to counterbalance the movement. In essence using joint cushioning. On the other hand, a roll landing is categorized by a forefoot touchdown followed by a forward roll

on the back. Roll landing principle is based on increasing the break distance by transferring vertical motion into horizontal motion. Also, the multiple contacts that are made and broken through the roll distribute the impact forces throughout the body rather then concentrating them at one point.

1.2.2 Robotic Software Strategies

Most of the initial work on humanoid falling was done by Fujiwara et al.[2, 16, 17, 18]. Fujiwara et al suggested that the damage to the whole body can be reduced by contracting and expanding the body length. Then, Fujiwara et al.[18] realized backward and forward falling motions using an optimal planning method. Similarly, Wang et al.[19] extended the work to whole-body optimal trajectories for minimizing damage. However, this motions are only effective when falling from a static standing position.

More recent work by Ogata et al. [20] proposed a detection algorithm based on experiential learning to distinguish between fall and no-fall condition. The algorithm is able to distinguish between disturbance of a steady walking gait and actually falling for a humanoid constrained to the sagittal plane. Ogata et al. decrease the damage to the robot by using a closed form solution to determine an optimum hand placement to minimize the angular velocity of the falling robot. Yun et al. [21], extended the work to a 3D scenario. He proposed the use of stepping to prevent falls once detected and if not possible use inertia shaping to change the falling direction to minimize impact velocity. Differently, Lee [3] proposed a controller algorithm to force the humanoid to always fall in its back as it was mechanically stronger to withstand impacts. He estimated the truck angular velocity required to orient the humanoid to fall on its back and then calculated the necessary joint accelerations to achieve the necessary trunk velocity.

All the control algorithms mentioned showed capable of minimizing the impact forces. However, they are aimed to mitigating humanoids falls from a pseudo-static standing position, not high impact falls from drop jumps. Further, the algorithms proposed only aim to decrease the damage to the robot. They do not consider readiness for the next action after impact. We are interested in not only landing safely from a drop jump but doing so controllably to transition to walking or running gait after impact.

1.2.3 Robotic Hardware

Most humanoid robots developed so far are stiff because it leads to good position control capabilities. However, they are also fragile and cannot handle dynamic interactions with the environment such as jumping [22]. Differently compliant low stiffness robots are better at absorbing large impact forces but suffer from inferior position position control capabilities. The use of compliant joints in the form of Series-Elastic-Actuation [23] and/or similar have become a popular method to protect the robot against impact [5, 6]. Radkhah et al.[24] showed that the shock absorption properties could be improved by tuning the actuators stiffness. By using softer springs the robot was dropped from 25 cm instead of 5 cm without reaching critical torque peaks at the transmission.

Joint compliance has been introduced in robotics in various ways. In [25] Niiyama and Kuniyoshi introduced compliance to their bipedal system via pneumatic actuators rather than

(a)

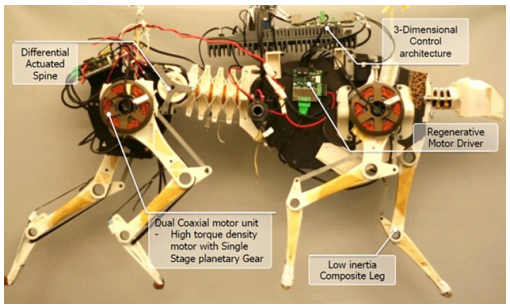

(b) (c)

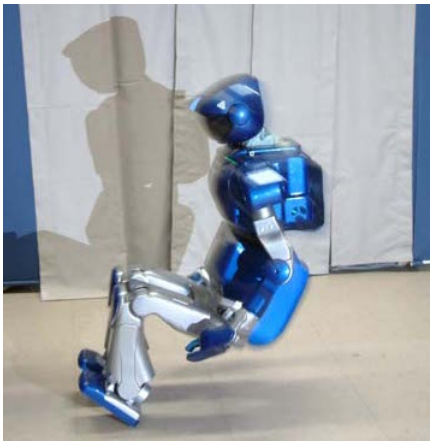

Figure 1.2: Existing Legged robots that have implemented software impedance rather than through physical elements. (a) MIT Cheetah uses impedance control [1], (b)HRP-2P robot falling [2], (c) ASIMO Robot. [3]

using spring like elements. This robot was capable of withstanding the impact from a 1 meter fall without breaking any components. Other common approaches are inspired by tendons in biological systems. Ananthanarayanan et al. [26] use of a tendon like element reduced the stress on the bone during a stride by up to 59%. Ito et al. and Dallali et al. proposed different elastic element arrangement to replicate antagonistic tendon layout in humans. Both showed a decreases in impact shock [4, 22]. Dallali et al. improved its leg shock absorbing capabilities by introducing impedance control.

Similar to the software strategies presented the mechanical strategies are targeted for mild interaction with the environment and fall short to mitigate the large impact forces of explosive maneuvers.

1.3 Problem Statement

In this dissertation we focus on the explosive motion of drop jumping. We define drops jumps as the action starting at a given height above the ground, followed by a free-fall phase, and terminating by landing on the ground on feet. As a goal we aim to achieve a controllable and

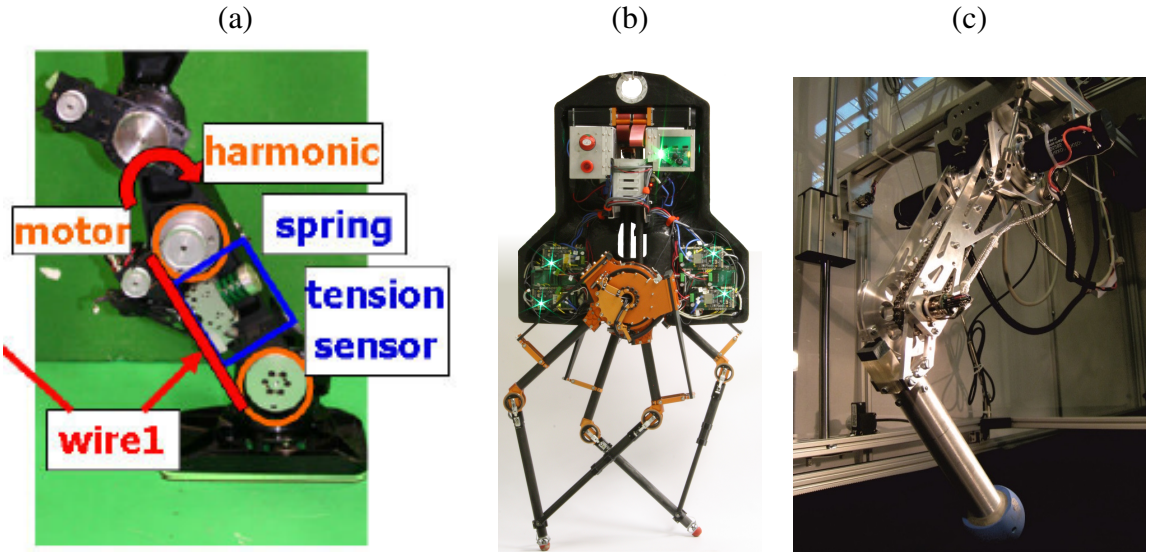

Figure 1.3: Existing legged robots that use physical elements to introduce compliance. (a) Tendon-driven and axial-driven hybrid humanoid leg [4], (b) ATRIAS [5] (c) Scarleth [6].

safe drop jumps from at least a second floor (≈3m high).

The problem of landing drop jumps and reducing impact forces is governed by the impulse-momentum theorem:

$$\underbrace{I}_{\text{Impulse}} = F \cdot \Delta t = \underbrace{M \Delta v}_{\Delta\text{Momentum}} \tag{1.1}$$

where F is the ground reaction force, Δt the length of time F is applied for, M the system's total mass, and Δv is the change in velocity of the system. By equation (1.1) the impulse (I) that the ground exerts on the object is equal to the change of momentum. For any object with a given mass, falling from an initial height h_0 above the ground, and with no external forces acting on it, the velocity of the object just before impact (v_{TD}) can be calculated in close form (equation (1.2).

$$v_{TD} = \sqrt{g \cdot h_0} \tag{1.2}$$

Assuming that the ground is rigid, upon impact it will bring the falling object to complete stop. The final velocity of the object (v_f) will be zero. Thus, the change in velocity (Δv) can also be calculated by

$$\Delta v = v_{TD} - v_f = v_{TD} - 0 = v_{TD} \tag{1.3}$$

Thus, we can conclude that for any given mass and height falling to a rigid ground the change of momentum and the impulse are constant. Further, from equation (1.1) we note that the product F and Δt is constant but their individual value are not. With the freedom on modifying their value maximizing Δt will explicitly minimize the reaction force F by the ground on the object. Two ways to minimize Δt are to minimize the deceleration $\dot{v}$ of the object as it comes to a rest and/or maximize the breaking distance. Therefore, to reduce the forces on a robotic system perform drop jumps we investigate methods to minimize $\dot{v}$ and maximize breaking distance.

In this work, we define a successful landing as one that minimize the risk of mechanical failure and disruption of momentum. This translates to ability to absorb the shock at landing, while maintaining readiness for the next action. We tackle the problem with a two prong approach. We investigate mechanical design and control strategies to achieve safe drop landings.

1.4 Contributions of this work

In this work we make the following contributions:

- We propose a novel design for adult human size robotic leg to be part of a bipedal robot, that extends the capabilities of existing legs to protect the integrity of all components from large impact forces.
- Demonstrate the need of a physical damping element to be able to perform controllable drop jumps. We showed in simulation the ability to land from drop jumps of 6m without bouncing.
- Implement an optimal impedance control to show a simple algorithm to successfully be capable of performing a controllable landing.
- An accurate 3D simulator of the robot was developed, including a detailed model nonlinear spring, damper and transmission. This tools should be of great utility for upcoming work.
- Build and test a prototype of the novel shin component of the leg that implements our proposed impact attenuator with a fiberglass leaf spring and active magneto-rheological damper.

Chapter 2

Mechanical Design

2.1 Design overview

The proposed High Impact Landing (HIL) leg (Figure 2.1) is designed with the aim of extending current bipedal systems' capabilities. Explicitly, HIL leg purpose is to robustly survive the impact of landing feet first from free-falls, and controlling the system energy to efficiently transition from landing to walking/running gaits. Contrary to classical legged locomotion systems we aim to maximize the energy losses and negative work upon impact with the ground so that we do not bounce. Additionally, our design is intended for the robot to be capable of impacting the ground with the knee joint as well as the foot. The design decisions where governed by the aim to maximize four functional requirements; agility, torque actuation, impact force attenuation and sensing.

HIL leg is designed primary to be a good shock absorber, but also has to be a good walker and runner. Thus, to leverage prior work in the research work on human walking and running we want to maintain a human form factor. The leg fully extended measures 1.24m from hip to foot. The total mass of leg is 11Kg, with weight primary concentrated at the hip. HIL was designed in mind to perform extreme agile maneuvers such as rolling. Thus, it has a large range of motion. Dimension of the leg and joint ranges are summarized in Table 2.1 and Table 2.2 respectively.

Table 2.1: Mechanical parameters of HIL Leg

	Length [m]	**Mass [kg]**	**CoM [m]**
Hip	–	5.04	–
Thigh	0.56	4.51	(0.13,-0.38,-0.15)
Knee	–	1.1	–
Shin	0.68	7.28	
Overall	1.24	14.03	(0.22,-0.40,-0.20)

(a) (b)

Figure 2.1: CAD model of (a) HIL leg and (b) bipedal configuration concept

2.2 Design requirements

Based on the literature review from section 1.2 and our problem statement we identified four functional requirements that our design has to fulfill. The requirements are: high agility, powerful, impact resistant, and controllable. For the robot to be capable of performing dynamic motions it has to be agile in terms of having a large range of motion and move fast. Explosive actions involve large amounts of energy, the robot has to be powerful to be able to generate enough energy to perform such actions. The main aim of this robot is to be able to withstand high impact. To be able to implement novel and complex feedback controllers on the robot we need to be able to accurately estimate the robot state. Therefore, sensors are important. Table 2.3 summarizes the functional requirements and their respective engineering specification.

2.3 Agility

Traditionally serial link robots have large distal link inertia because actuators are commonly located at the joints. Thus, they have high energy requirements to achieve fast leg motion with high acceleration [27]. We co-axially aligned two actuators with the hip axis, far from the end effectors to minimize the rotational inertia of the legs, similar to [1][6][5]. Thus, effectively

Table 2.2: Range of Motion of HIL Leg Joints

Joint	Min.	Max.	Units
Hip	-100	120	degree
Knee	-95	0	degree
Shin	0	7.5	centimeter

Table 2.3: Functional and user requirements conversation to engineering specifications

Functional Requirements	Operational Requirements	Engineering Specs.
Agile	Large joint range	$\alpha_h \in [-90, 90]$
		$\alpha_k \in [0, 90]$
	Low inertia	Minimize
	Lightweight	$\leq 20kg$
Powerful	High torque	$\geq 1000Nm$
Impact resistant	Physical and virtual protection	$\geq 3m$ drops
Controllable	Good state estimation	≥ 19 bit resolution
	Low latency communication	≥ 100Hz

moving the center of mass (CoM) closer to the hip axis that aids to keep leg inertia minimal. CoM is 15.3cm from the center of rotation. Additionally, as inferred from equation (1.1) lower distal mass is advantageous for minimizing impact impulse. A cross-sectional view of the hip joint is shown in Figure 2.2.

The kinematic configuration of system achieves a large range of motion. The leg can be swing $\Theta_{\text{hip}} \in -100°, 120°$ about the hip axis and flexion $\Theta_{\text{knee}} \in -95°, 0°$ about the knee axis. In a fully extended configuration the leg measures 1.24m from hip to foot.

2.4 High power density

The nature of the task to withstand and absorb the shock of high impact collisions requires large joint actuation to counter act the reaction forces to prevent the leg from collapsing to the ground. To meet this need we compared four motors; two motors from Allied Motion and two from RoboDrive. Table 2.4 summarizes the specs of theses motors. To actuate the hip and knee joints we selected a RoboDrive 115x25 motors capable of providing 5.4Nm of continuos and 18Nm peak torque. Both the hip and knee motor torque output are augmented by a harmonic drive. The hip joint is directly driven from the harmonic drive output, while an additional belt transmission is used to drive the knee joint. A harmonic drive was selected over a pulley based transmission. Harmonic drives are simpler to install than pulley systems, no consideration of cable tensioning is required. Also, pulleys occupy a bigger volume. Though sufficient space exists to replace the knee belt drive with pulley system, the leg's volume would need to be increased to add a pulley transmission for the hip joint. A harmonic drive with 50:1 gear ratio was selected over

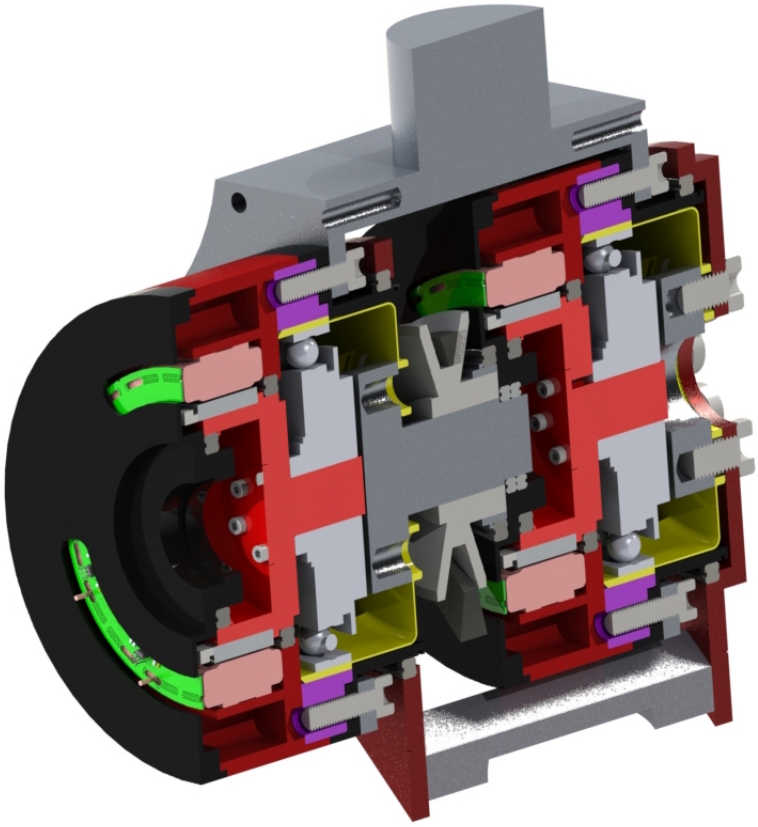

Figure 2.2: Cross-sectional view of 3D CAD rendering of hip joint

the desired lower 30:1 ratio because of the rated limit repeated peak torque. Highest rated 30:1 harmonic could only handle peak torques of 200Nm, while the selected harmonic drive 1235Nm.

2.5 Impact Force Attenuation

The novelty of the design lies within the shin and the additionally degree of freedom in it (Fig. 2.6). Inspired by power stilts [28]the shin is capable of undergoing a large deformation without failing due to the large fiberglass leaf spring that joins the knee and the foot. The leaf spring is a stiffening nonlinear spring, a desirable characteristic. A fiberglass leaf spring was chosen over a common metal helical spring as it has been shown in [29] to be better at returning energy. The deformation is constrained by the shin linkage mechanism, improving the measurement accuracy of the foot position.

Minimizing energy losses after impact is desirable for some actions such as running and walking. However, for landing the opposite is desirable. To reduce the strain on the mechanism and improve post impact controllability maximizing energy loss is desirable. To control the energy dissipation of the leg upon impact we drew inspiration from active shock absorbers in motorcycles and cars that place a Magneto-Rheological(MR) Damper in parallel to a spring.

ID Number	ILM115-50	ILM115-25	MF0150010	MF0150025
Manufacturer	RoboDrive	RoboDrive	Allied Motion	Allied Motion
Peak/Stall Torque [Nm]	40	18	19.4	50.9
Continous Stall Torque [Nm]	11.2	5.4	3.5	9.1
Peak Current [A]	20	20	56.7	130.5
Voltage [V]	48	48	48	48
No-load speed [rpm]	650	1300	1293	1775
Weight [kg]	2.17	1.2	1.12	2.73
Dimensions [mm]	115x50	115x25	170x13.06	170.29.06

Table 2.4: Off-The-Shelf Motor comparison. RoboDrive ILM115-25 was selected.

In our design we use the MR damper RD-8040-1 developed by Lord Corporation. The use of MR dampers in prothetic limbs has being growing in popularity [30, 31], but to the best of our knowledge have not being ported to legged robotic systems. Using a variable stiffness shin we control the energetics of impact landing. It provides the ability to handle the energy storage and dissipation to control the bouncing after impact. It also allows us to protect the motors from reaching peak torques by managing the force transfer.

Despite MR dampers being an easy method to control impedance in the leg, it has some drawbacks. There are few MR dampers options commercially available. The RD-8040-1 was the only one that fitted our sizing requirements and it has a small 7.5cm maximum stroke limiting the shin's deformation. Thus, it reduces the amount of energy it can dissipate in one compression. Also, the iron particles of the MR Fluid significantly increase the shin's mass. The MR dampers accounts for 83% of the total mass of the shin.

2.5.1 Magneto-Rhelogical (MR) Dampers

MR dampers (see Figure 2.4) resemble in size and operation to regular dampers. The difference is the viscous liquid inside the damper casing. MR fluids are free flowing liquids with similar consistency similar to that of motor oil but with iron particles in it. In the presence of an applied magnetic field, the iron particles acquire a dipole moment aligned with the external field which causes particles to form linear chains parallel to the field. This phenomenon solidify the suspended iron particles and restrict the fluid movement. Consequently, yield strength is developed within the fluid. The degree of change is related to the magnitude of the applied magnetic field, and can occur only in a few milliseconds [7].

MR fluids have a wide range of applications such as: dampers, shock absorbers, rotary brakes, clutches, prosthetic devices, polishing and grinding devices. However, major drawbacks that hinder MR fluid damper applications are their nonlinear force/displacement and force/velocity characteristics. Accurate models of the MR fluid are required to be able to design proper control algorithms [7].

2.6 Controllability

To diminish controllability and state estimation error the robotic leg has several sensors attached to it. A 20bit resolution magnetic rotary encoders to measure the hip and knee angles. Each motor has a hall effect sensor and a 13bit resolution magnetic encoder. The spring deflection and damper compression are measured through the relation with the shin rotary joint (see Figure 2.6. It is measured by an absolute optical encoder with a 19bit resolution. Additionally, a limit switch is placed at the bottom of the foot to detect contact with the ground.

Table 2.5: HIL robot sensors table

Measurement	**Sensor**	**Manufacturer**	**Model**	**Resolution**
Hip angle	Magnetic rotary encoder	Renishaw	Aksim	20bit ($\pm 0.1°$)
Knee angle	Magnetic rotary encoder	Renishaw	Aksim	20bit ($\pm 0.1°$)
Spring deflection	Optical rotary encoder	Dynapar	AD35	19bit ($\pm 0.35°$)
Motor rotor angle	Magnetic rotary encoder	Renishaw	RMB30	13bit $\pm 0.5°$)
Motor rotor angle	Hall effect	RoboDrive	–	
Ground contact	Limit switch	Sparkfun	–	

2.7 Discussion

The final proposed design meets 6 of the 8 the engineering specification required to meet our desired functional requirements. Table 2.3 summarizes the demanded engineering specifications and the achieved specifications. The two 13 bit encoders are used for low level control of the motors and do not measure the joint angle. Thus, they do not violate the encoder's specification of least 19 bit resolution. Our design outputs 100Nm less than that desired torque. To achieve the desired 1000Nm torque actuation, the motor size has to be increased as well as the transmission gear ratio. Increasing the harmonic drive ratio diminish the performance of the leg due to the exponential increase in reflective inertia.

There are still aspects of the design that can be improved. For instance, adding accelerometers will provide better state estimation during all phases of a drop jump. The hollow square tube link supporting the MR damper should be replaced with a solid Aluminium 7075-T6 link to address the weak point identified in section 4.3. Finally, either a clutch to engage the damper at will or using a different damping element should be implemented to mitigate the issues of the high passive damping coefficient of the MR Damper.

Table 2.6: Required and achieved engineering specifications

Required Eng. Specification	**Achieved Specification**
$\alpha_h \in [-90, 90]$	$\alpha_h \in [-100, 120]$
$\alpha_k \in [0, 90]$	$\alpha_k \in [-95, 0]$
	$1.390kg \cdot m^2$
$\leq 20kg$	$15.49kg$
$\geq 1000Nm$	$900Nm$
$\geq 3m$ drops	6m in simulation, not tested in hardware
≥ 19 bit resolution	19bit resolution joint encoders
≥ 100Hz	N/A

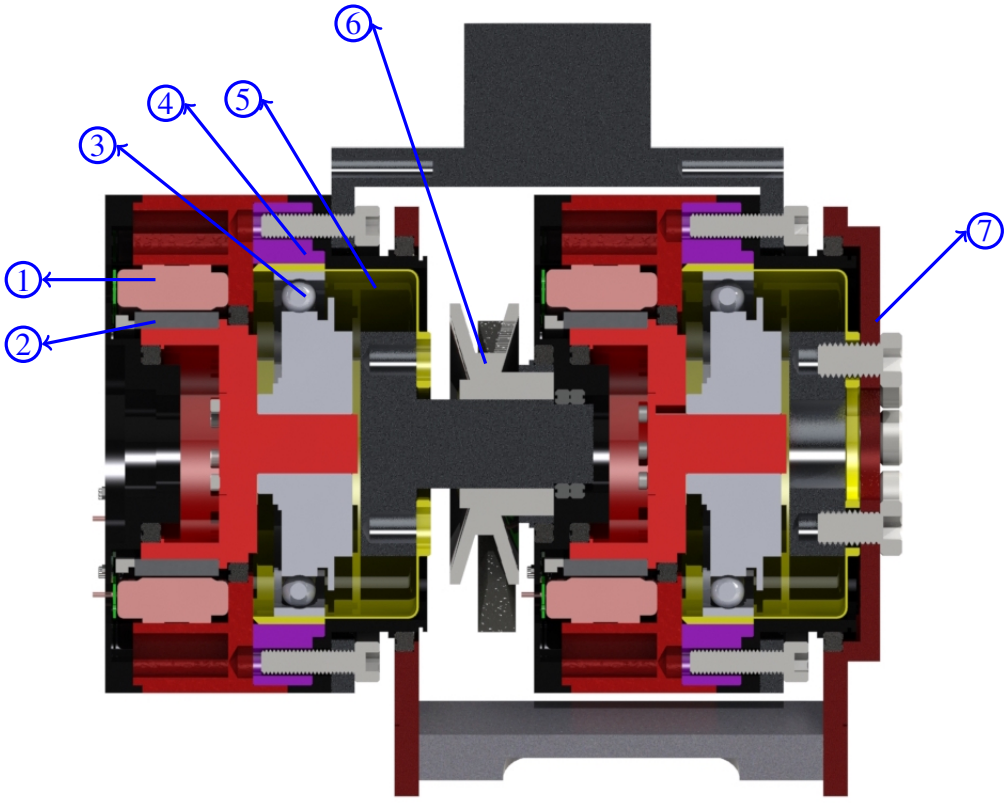

Index No.	Name
1	Motor stator
2	Motor rotor
3	Harmonic Drive wave generator
4	Harmonic Drive circular spline
5	Harmonic Drive flexible spline
6	Knee joint sprocket output
7	Hip joint output

Figure 2.3: Cross-sectional view of 3D CAD rendering of hip joint

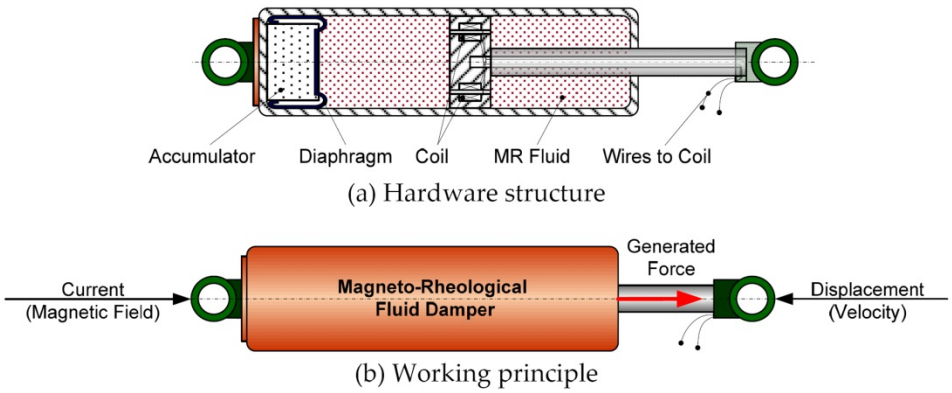

Figure 2.4: Schematic of general configuration of a MR fluid damper [7]

Figure 2.5: 3D CAD exploded view of HIL thigh leg section

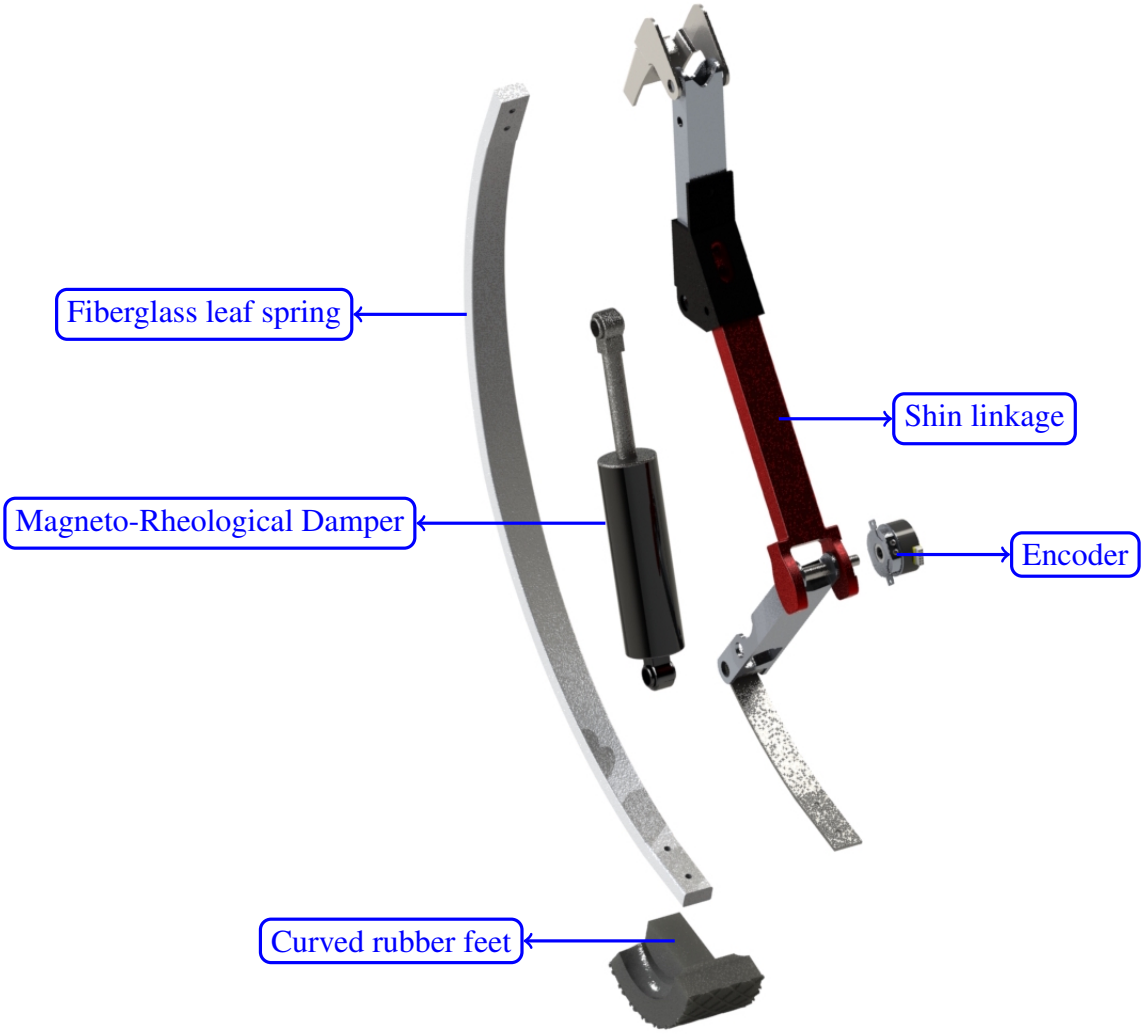

Figure 2.6: 3D CAD exploded view of HIL shin leg section

Figure 2.7: Picture of prototype built of HIL shin leg section

Chapter 3

Model & Simulation

3.1 Simscape Multibody Model

MathWorks MATLAB/Simulink Simscape Multibody toolbox provides a multibody simulation environment for 3D mechanical systems [32]. Simscape Multibody formulates and solves the equations of motion for the complete mechanical system. A powerful feature is the capability of importing complete CAD assemblies, including all masses, inertias, joints, constraints, and 3D geometry, into your model. An automatically generated 3D animation lets you visualize the system dynamics. Based on the leg design presented in Section 2 a model was build in Simscape (see Figure 3.1).

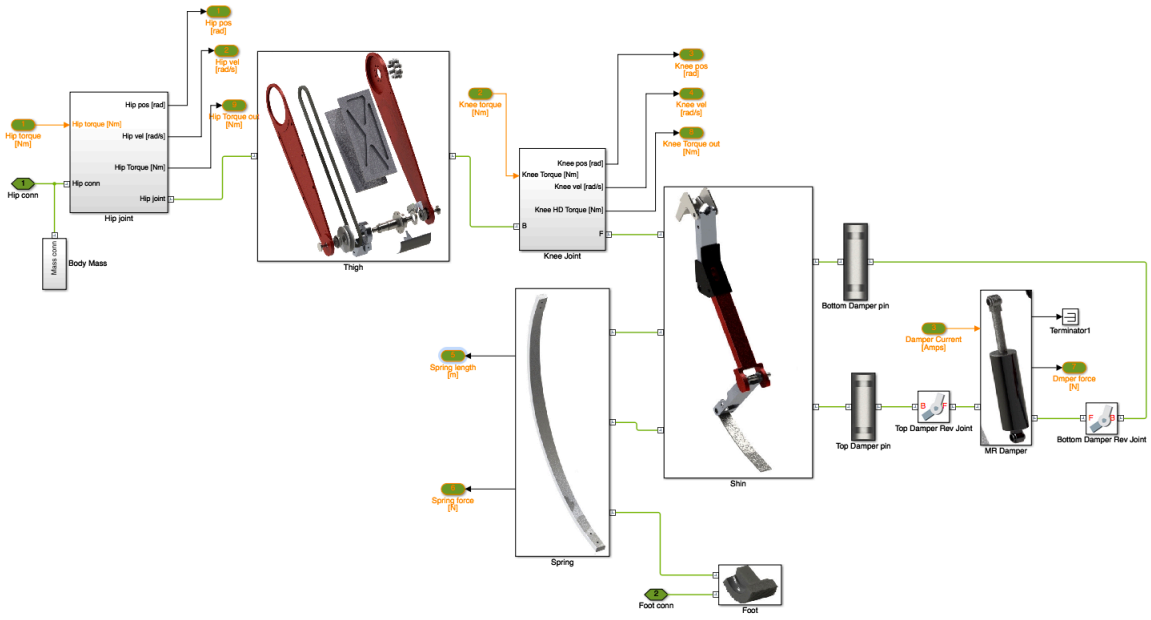

Figure 3.1: Screenshot of HIL leg model implementation in Simscape

The model is represented in a floating based coordinated system. The underlying model is a 2 joint serial open kinematic chain with a spring and damper in parallel at one the links. The

nonlinear spring force is given by equation (3.1) [33]. Where w, h, and L are the width, height and length of the leaf spring, E is the modulus of elasticity of fiberglass, and Δx is the spring deflection.

$$F_{\text{spring}} = \frac{16Ewh^3}{L^3}\Delta x \tag{3.1}$$

Two models of the MR damper were used; a simple linear force-velocity relation and a highly nonlinear force profile based on a hysteretic model [7]. The simple model is represented by equation (3.2).

$$F_{\text{damper}} = B\dot{x} \tag{3.2}$$

where B is a damping coefficient and $\dot{x}$ is the damper compression velocity. The hysteretic model (Figure 3.2) is represented by the equations:

$$F = c\dot{x} + kx + \alpha z + f_0 \tag{3.3}$$
$$z = \tanh(\beta\dot{x} + \delta \text{sign}(x)) \tag{3.4}$$
$$c = 1929i + 1232 \tag{3.5}$$
$$k = 1700i + 5100 \tag{3.6}$$
$$\alpha = 244i^2 + 918i + 32 \tag{3.7}$$
$$f_0 = 18i + 57 \tag{3.8}$$
$$\beta = 100 \tag{3.9}$$
$$\delta = 0.3i + 0.58 \tag{3.10}$$

where c and k are the viscous and stiffness coefficients; α is the scale factor of the hysteresis; z is the hysteretic variable given by the hyperbolic tangent function; f_0 is the damper force offset;β, δ are the model parameters identified experimentally; and i is the current supplied to the damper.

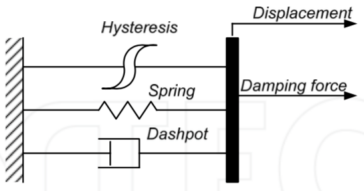

Figure 3.2: Hysteretic model of a MR Damper

The inefficiency and reflective inertial effects of the harmonic drive transmission are also modelled. Figure 3.3 is a screenshot of the transmission model implementation in Simscape. Similarly, the motor's rotor reflective inertia and damping are modeled as shown in Figure 3.4. The model parameters (mass, dimension, inertias, CoM locations) obtained from the 3D CAD model are summarized in Table 2.1. A boom is also modeled to constrain the motion of the leg to the sagittal plane.

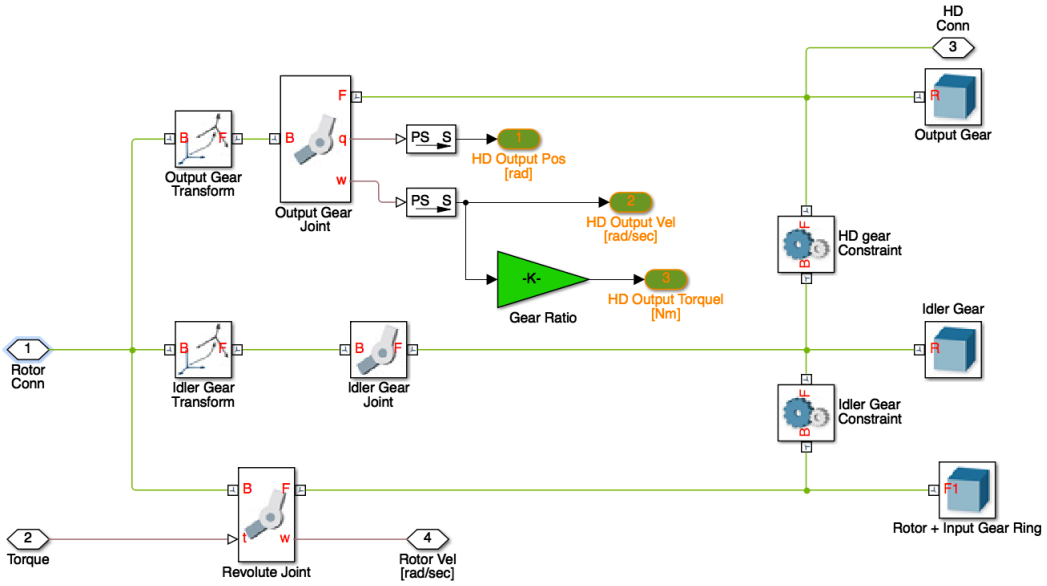

Figure 3.3: Screenshot of Harmonic Drive implementation in Simscape

3.2 Impact Dynamics

Simscape has a poor capability of resolving impacts. Thus, a more comprehensive model of the ground reaction forces is implemented. Collision between the ground and foot are modeled as point elastic collisions [34]. At the point of contact a ground reaction force $\vec{F}_{\text{GRF}}$ is exerted by the ground on the robot's foot. Resolving the dynamics with the additional external force on the system will generate the different effect on the joints. We assume point feet and that contact happens at a discrete point between the foot and ground. The force $\vec{F}_{\text{GRF}}$ is divided into its normal component F_N and tangential component F_T relative to the ground surface as shown in Fig 3.5.

F_N is calculated by the discontinuous equation:

$$F_N = \begin{cases} y \cdot k_{g,y}(1 - \frac{\dot{y}}{v_{g,y}}) & \text{if } \frac{\dot{y}}{v_{g,y}} < 1 \\ 0 & \text{otherwise} \end{cases} \tag{3.11}$$

where y and $\dot{y}$ are the vertical distance and velocity of the foot relative to ground respectively, $k_{g,y} = M_t/0.01\,[N/m]$ is the vertical ground stiffness, M_t is the robots total mass, and $v_{g,y} = 0.03\,[m/s]$ is the maximum relaxation speed of the vertical ground interaction.

While the foot is in contact the tangential force

$$F_T = F_{\text{static}} + F_{\text{kinetic}} \tag{3.12}$$

the sum of the static and kinetic friction. Note that since F_{static} and F_{kinetic} are defined as discontinuous function either the foot is sticking to the ground (i.e. $|F_{\text{static}}| > 0$ and $|F_{\text{kinetic}}| = 0$) or the foot is sliding (i.e. $F_{\text{static}} = 0$ and $|F_{\text{kinetic}}| > 0$). Static friction force is given by:

$$F_{\text{static}} = \begin{cases} -x \cdot k_{g,x} \left[1 + \text{sign}(x \cdot k_{g,x}) \frac{\dot{x}}{v_{g,x}}\right] & \text{if } |F_R| > \mu_{stick} F_N \\ 0 & \text{otherwise} \end{cases} \tag{3.13}$$

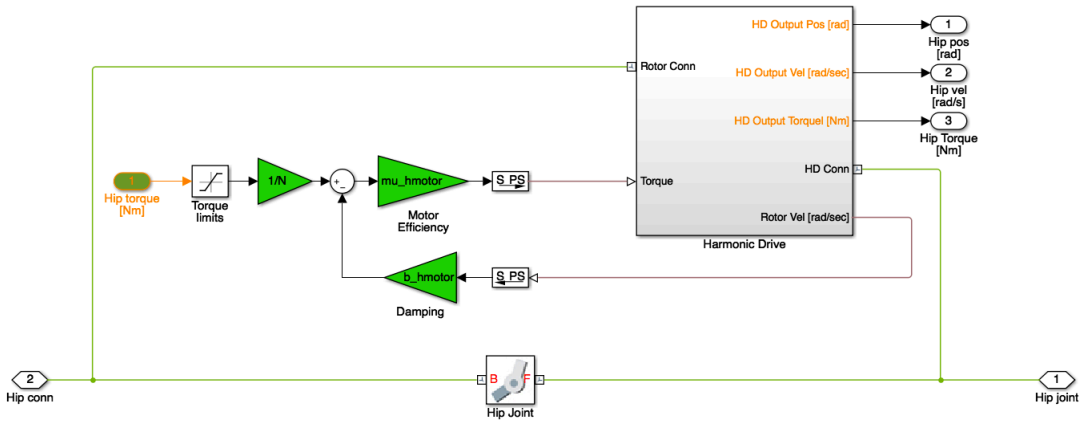

Figure 3.4: Screenshot of motor model implementation in Simscape

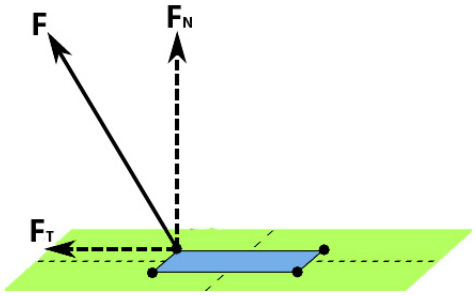

Figure 3.5: Diagram of contact forces

where x and $\dot{x}$ are the horizontal distance and velocity of the foot relative to initial point of impact with the ground respectively, $k_{g,x}$ is the horizontal ground stiffness, $\mu_{stick} = 0.9$ is the stiction to sliding transition coefficient, and $v_{g,x} = 0.03\,[m/s]$ is the maximum horizontal ground interaction relaxation speed. Kinetic friction force is given by:

$$F_{\text{kinetic}} = \begin{cases} -|\vec{v}| \cdot F_N \cdot \mu_{\text{kinetic}} & \text{if } |\vec{v}| < v_{\text{tresh}} \\ 0 & \text{otherwise} \end{cases} \tag{3.14}$$

where $\vec{v} = [\dot{x}, \dot{y}]^T$, $\mu_{\text{kinetic}} = 0.8$ kinetic friction coefficient, and $v_{\text{tresh}} = 0.01\,[m/s]$ the sliding to stiction transition velocity limit.

As a measure of correctness we employed a second method to calculate ground reactions forces from Newton's 2nd law. We assume that only GRF and weight act on the systems center of mass (CoM) and thus

$$F_N = M_t \cdot g - M_t \ddot{y}_{\text{CoM}} \tag{3.15}$$

where $g = 9.81 m/s$ the acceleration due to gravity and $\ddot{y}_{\text{CoM}}$ is the systems center of mass measured vertical acceleration.

3.3 Optimization

Systems that have multiple phases of continuous dynamics separated by discrete transitions maps are called hybrid systems. A system that experience a collision can be usually represented as a hybrid system [35]. For our robotic leg falling and landing on the ground the continuous phases are the free fall motion (pre-impact) and the compression/decompression while in contact (post-impact). A discrete transition (impact with ground) joins the two continuous phases.

The discrete transitions of hybrid systems make it unsuitable to wrap the different phases inside a big dynamic simulation/function and solve using the commonly used optimization algorithms (e.g. FMINCON[32], SNOPT[36], IPOPT). This is because the underlying algorithm is based in gradient-descent that typically expect continuous and smooth functions. The discrete transition make the dynamics non-smooth.

To obtain optimal open loop landing gaits we explore three methods to handle hybrid systems: multi-phase, through-contact, and derivative/gradient-free methods. Multi-phase methods require a priory sequence of phase transition. In our case this would be a prior sequence of contacts locations and time. For each phase of continuous dynamics an independent optimal control problem is formulated and solved. A set of boundaries constraints are set to ensure the correct transition between phases. This method has been widely used to solve optimal control probles that involve impacts such as; finding walking gaits for bipeds [37] or minimizing damage from falling a standing position [18, 38].

Through-contact methods represent the system dynamics in floating based coordinate system and handle contact implicitly through linear complementary constraints [39]. Thus, the system is no longer represented as a hybrid system. Contact forces are treated as optimization parameters. This method will search for optimal control inputs as well as optimal contact scheduling. Thus, it will be able to determine what is the best landing motion. However, reformulating the problem to fit this framework is not simple.

Derivative-free optimization methods, as the name states do not use information of the derivative to drive the system to an optimal solution. Thus, it is capable of handling the discontinuities of the dynamics as well as discontinuities in the cost function. There are several families of derivative-free methods. We chose to focus on *Covariance Matrix Adaptation Evolution Strategy* (CMA-ES)[40] a type of evolutionary optimization algorithm. This family of algorithms is broadly based on the principle of biological evolution, namely the repeated interplay of variation and selection. In each iteration candidate solutions are generated in a stochastic way from the current parental individuals. Then, some individuals are selected to become the parents in the next generation based on their objective function value. Evolutionary algorithms have been successfully used for trajectory generation of walking bipeds[41, 42], however they have high computational time.

3.3.1 Optimal Control Problem Formulation

An optimal control problem can be posed to find an admissible time history of the control input $\mathbf{u}(t), t \in [t_I, t_F]$ as:

$$\min_{\mathbf{y},\mathbf{u}} \mathbf{J}(\cdot) = \mathbf{\Phi}\left(\mathbf{y}_F\right) + \int_{t_0}^{t_F} \mathcal{L}\left(\mathbf{y}(t)\right)\, dt \tag{3.16}$$

subject to:

$$\mathbf{H}\left(\mathbf{y}(t_I), \mathbf{y}(t_F)\right) = 0 \tag{3.17}$$

$$\mathbf{G}\left(\mathbf{y}(t), \mathbf{u}(t)\right) \leq 0 \tag{3.18}$$

where $\mathbf{\Phi}(\cdot)$ is the terminal cost, $\mathcal{L}(\cdot)$ is the running cost. $\mathbf{H}(\cdot)$ are equality constraints that enforce system dynamics and boundary conditions. $\mathbf{G}(\cdot)$ are nonlinear inequality constraints that define joint angle and torque limits. For the problem to be solvable we assume that $\mathbf{J}(\cdot), \mathbf{H}(\cdot), \mathbf{G}(\cdot)$ are all smooth functions. Direct optimization of the value of $u(t)$ performs well when dynamic constraints are smooth and continuous. Optimization of a policy parameters that will define the profile of $u(t)$ is better suited for our problem. In this case the control inputs will be a function of the parameters y (i.e. $u(t, y)$). This type of problem can be solved using both multi-phase gradient descent and gradient free based algorithms.

Chapter 4

Experimental Results

4.1 Benchmark Simulated Drop Test

As a benchmark to determine the performance of different landing strategies and the use of a semi-active physical damper, we simulated two extreme case drops from 3m in the Simscape model. Case one is a stiff leg that requires excessive amounts of force to bent the joints and no elastic or damping element in the shin is implemented. Case two is a model with extremely compliant joints and only spring in the shin, no damper. In the stiff case as expected there is no flexion of the joints. Consequently, the GRF is extremely large around 60000N (see Figure 4.6). This will certainly break the robot. In the compliant case GRF are minimum however the landing is uncontrollable. In Figures 4.1 and 4.1 we see that upon impact the leg collapse to the ground. The CoM ends up at the floor level indicating the robot fell down. Also, there is a large change in the x-position of the foot due to the rotation of the body after it bounces of the ground. The rotation of the leg can be partly explained by the momentum difference between the payload mass traveling downwards while the foot is traveling upwards. Clearly from these two test there is a lot of room to improve.

4.2 Optimal Impedance control

Virtual impedance control is a simple method to mimic the natural compliance and damping in human's joints. Similar to the knee cushioning strategy used by humans where joint stiffness and damping are set pre-impact, we can set the proportional and derivative gains of impedance control. If the impedance control follow the laws

$$\tau_h = k_{p_h}(\alpha_h - \alpha_{h,0})k_{d_h}\dot{\alpha}_h \tag{4.1}$$

$$\tau_k = k_{p_k}(\alpha_k - \alpha_{k,0}) + k_{d_k}\dot{\alpha}_k \tag{4.2}$$

where, τ_h hip torque [Nm], τ_k knee torque [Nm], k_{p_h} hip stiffness coefficient [N/m], k_{d_h} hip damping coefficient [Ns^2/m], k_{p_k} knee stiffness coefficient [N/m], k_{d_k} knee damping coefficient [Ns^2/m], $\alpha_{h,0}$ initial hip angle [rad], $\alpha_{k,0}$ initial knee angle [rad] then the gains to set are $k_{p_h}, k_{d_h}, k_{p_k}$ and k_{d_k}. Determining the optimum values for the virtual impedance gains and

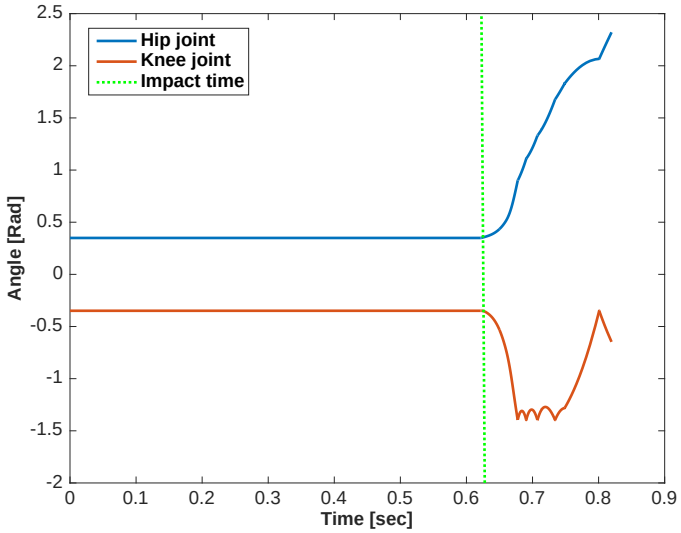

Figure 4.1: Joint trajectory for a simulated drop jump from 3m with a very compliant robot

damper coefficient is a non-trivial task. From observing humans land, we know that the landing shape plays a big role on the impact force magnitude, because the landing configuration has a large effect of how the passive dynamics of the system will evolve post impact. The HIL leg shape is determined by α_h and α_k. The landing shape and the internal parameters together define a landing configuration. A constrained nonlinear optimization problem similar to that described in Section 3.3.1 was formulated to find the optimum landing configuration:

$$\min_{Kp_h, Kd_h, Kp_k, Kd_k, B0} \mathbf{J_1}(\cdot)$$

subject to:

$$\alpha_{h,\min} \leq \alpha_h \leq \alpha_{h,\max}$$
$$\alpha_{k,\min} \leq \alpha_k \leq \alpha_{k,\max}$$
$$\tau_{h,\min} \leq \tau_h \leq \tau_{h,\max}$$
$$\tau_{k,\min} \leq \tau_k \leq \tau_{k,\max}$$

where the cost function (Eqn. 4.3) minimizes peak GRF, bounce height and control effort. Notice, that the peak GRF is expressed as a terminal cost value. The knee travel distance is directly correlated to the breaking distance. From the impulse momentum equation the increase in break distance implicitly decreases GRF. Thus, the cost function also maximizes knee joint deflection. Additionally, to penalize bouncing post impact the vertical foot position is minimized.

$$\mathbf{J_1} = \max(GRF.z) + \int_{t_{TD}}^{t_F} w_1 P_{ft,z}^2 - w_2 \theta_k^2 + u^T W u \, dt \tag{4.3}$$

t_{TD} Touchdown time
t_F Final simulation time
P_{ft} Position of foot, $[P_{ft}^x, P_{ft}^y, P_{ft}^z]^T$

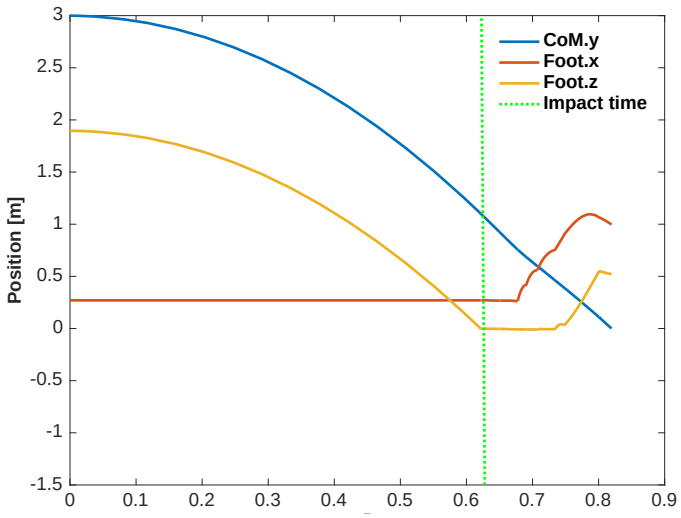

Figure 4.2: Foot position trajectory for a simulated drop jump from 3m with a very compliant robot

4.2.1 Optimization Results

The constrained nonlinear optimization problem is solved using CMA-ES in Matlab. The optimization was performed for a range of initial jump heights $y_0 \in [1.5, 6]m$. Figure 4.3 shows the optimization results. For all five variables there is a sudden change in the trend of values after $y_0 = 4m$. The change can be explained by considering that larger initial potential energy leads to larger impact velocities. Consequently, post impact joint velocities will also be larger. Since, we defined input laws that are functions of position and velocity the motors will be saturated if the gains are not decreased. Also, since there is more energy to dissipate to prevent the leg from bouncing the damper has to do more negative work.

It is important to point out the large order of magnitude difference between the physical damper and the virtual damper at the joints. It is clear that most of the work that prevent the bounce is done by the shin damper. Also, we notice that for drop jumps from lower than $3m$ there is no hip actuation. The hip actuation will push the leg down on to the ground. This is only required when there is more energy in the system that the shin alone can dissipate.

4.2.2 Simulated Drop Test Results

The impedance control with optimum gains was tested on the Simscape model. Here we highlight two drop tests performed. In both test the optimal impedance control was implemented and the leg was dropped from 3m. The tests differ in that one has the physical damper deactivated. In all subsequent plots we denote the results as ”Optimal w/o damper” and ”Optimal w/ damper” to differ the two tests.

As shown in Figure 4.4 the physical damper is required to perform a controllable landing without bouncing. Without the damper only 1/3 of the initial energy is dissipated causing the leg to bounce back to a height of 2 meters. After the bounce the leg manages to stick the landing and dissipate all the remaining energy of the system. Figure 4.5 shows the joint trajectory for both

simulated drop tests. The joint trajectory of that with the physical damper is better with only one rapid change in joint position. Repetitive impulses causing sudden jerk motion in the joint is not desirable. The landing motion with the physical damper mimics that of a human performing a precise landing, that is bending the knee to extend the breaking distance.

The GRF for both tests are shown in Figure 4.6. Comparing the GRF better demonstrate the benefit of having the physical damper in place. Compared to the rigid case using the optimal impedance controlled managed to significantly decrease the peak GRF. Adding the damper further decreased the GRF by 7500N. This is significant because it implicitly also decreases the joint torques to be below the rated limit of the harmonic drive (see Figure 4.7). With the addition of the damper the benefit of a long rising time gained through the elastic element is lost. However, the benefit of adding damper to reduce GRF is greater than having a long rise time.

The results presented in this sections show that electric motors alone do not have enough power to handle large impact forces. The introduction of a physical semi-active damper is useful as it took over most of the work to dissipate a jumps energy, making it possible to perform a landing without bouncing.

4.3 Preliminary Hardware Drop Test

With the bottom half of the HIL leg build (see Figure 2.5) we conducted three sets of drop test to evaluate the mechanical design. For all test the the HIL leg was constrained to a linear vertical motion by attaching it to a rail. A deadweight of 15kg was added to the top of the shin at the knee joint to simulate the weight of the rest of the leg and payload. All drop test where recorded with Edgetronic high speed camera at 600 fps.

Test set (1) consisted on dropping the HIL shin without the MR-damper from a range of heights 1 to 6ft. This test served as the performance benchmark to improve upon. In all drop test below 3ft there were no significant bounces post impact. They were all in the order of a couple inches. Also, there was almost no compression of the spring post impact. We identify the drop test results from the upper bound of 6ft (see Figure 4.8) to describe the general behavior for drop jumps from above 3ft. The HIL shin bounced 4 times before coming to a rest. On the first touch down the HIL shin bounced back to 3ft high , on the second only to 1ft, and on the remaining bounces only a couple inches.

Test set (2) consisted on dropping the HIL shin with the MR-damper from a range of heights 1 to 6ft. No current was supplied to the MR-damper, so that only the passive dynamics of the damper would affect the systems behavior. In all drop test below 4ft there were no bounces and no compression post impact. Again we pick the test results from the upper bound of 6ft (see Figure 4.9) to describe the general behavior for drop jumps from above 4ft. The HIL shin bounced only once to a height of 5 inches before coming to a rest.

Test set (3) was almost identical to test set (2) they only differed that a 2A current (the maximum allowed) was supplied to the MR-damper. There was no visible difference between the results of test (2) and (3). This suggests that the system is over damped in test set (2). Implying that the MR-damper has a large damping effect in its passive state (no current supplied) that is more than required. Thus, the MR-damper capability to change its damping factor would only be useful if a larger load is applied to it. This can be done by either increasing the payload mass

or the initial drop height. A drop test was performed with double the payload mass, but one of the shin linkage was not able to support the load and bended (see Figure 4.10).

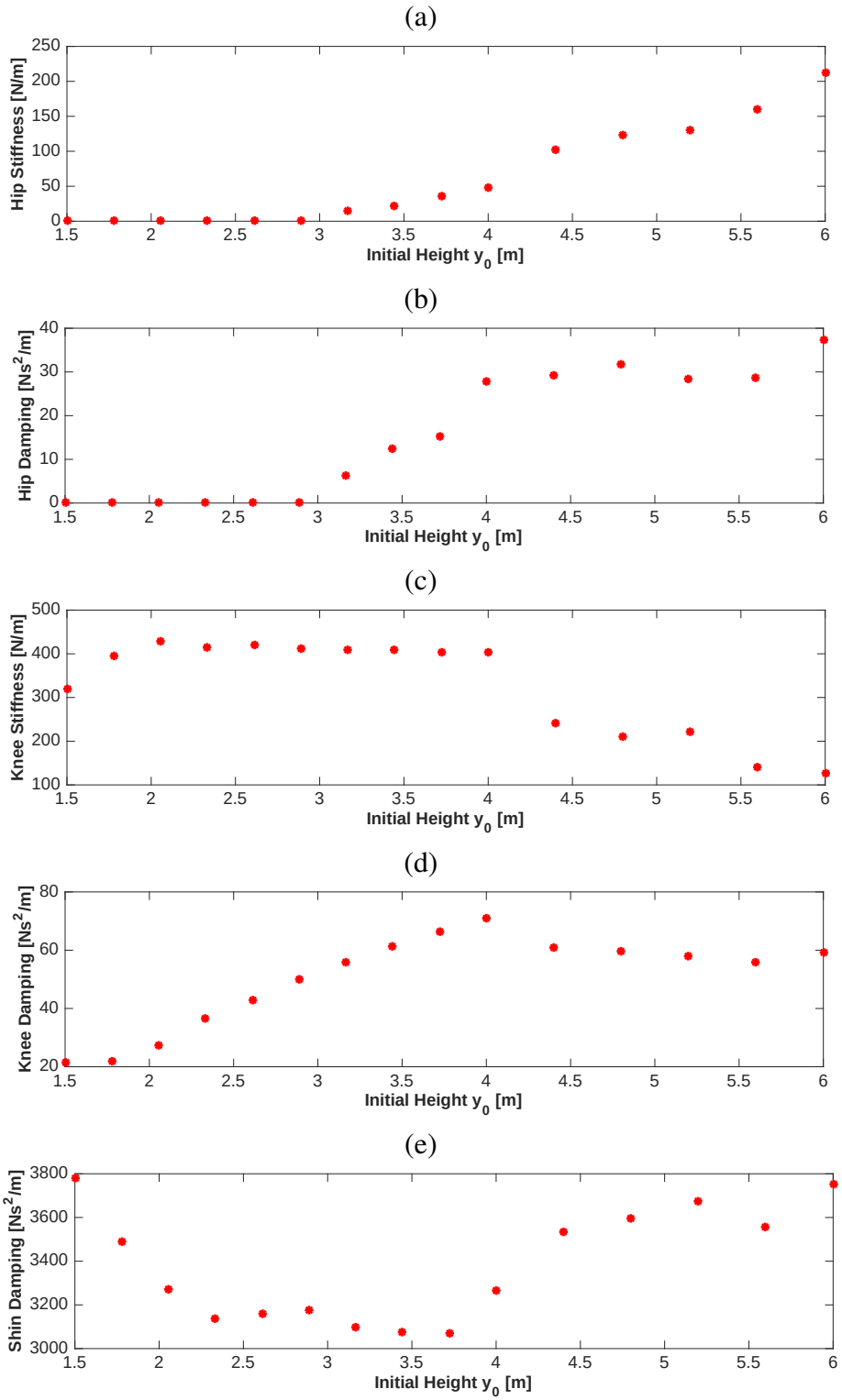

Figure 4.3: CMA-ES optimization results for; hip (a) stiffness, (b) damping, knee (c) stiffness, (d) damping, and (e) shin damping coefficients

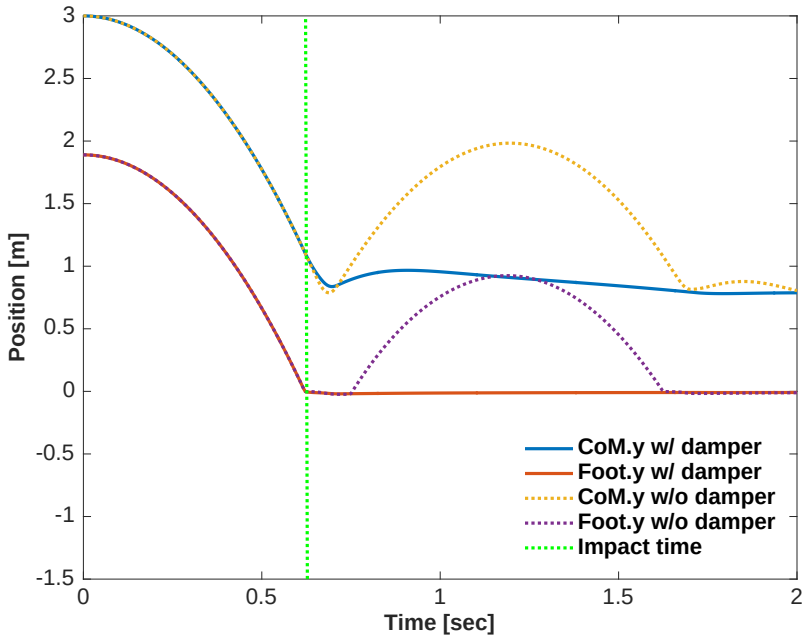

Figure 4.4: Foot position and CoM trajectory for a drop jump from 3m with optimal impedance gains and semi-active physical damper

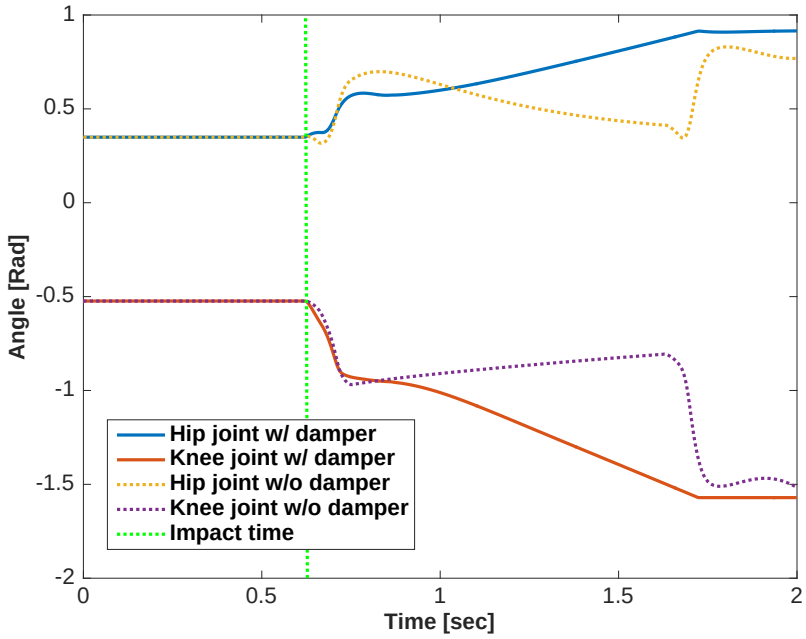

Figure 4.5: Joint angle trajectory for a drop jump from 3m with optimal impedance gains and semi-active physical damper

(a)

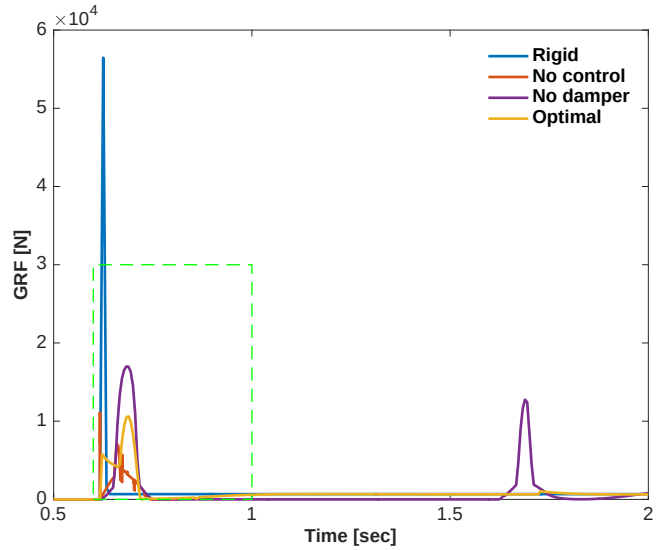

(b)

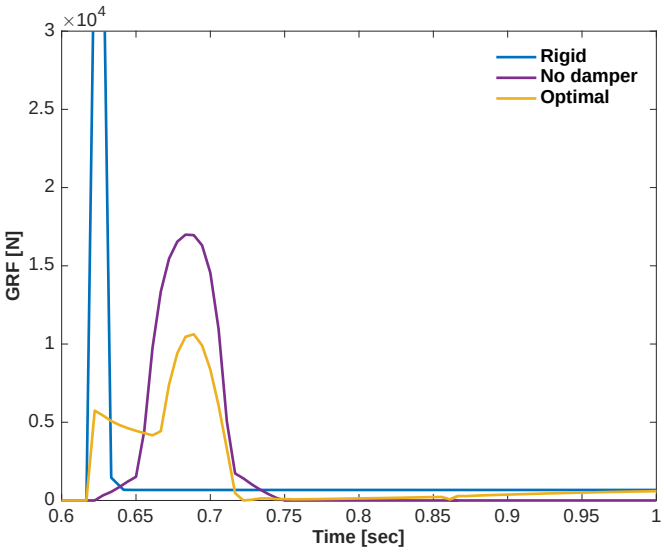

Figure 4.6: (a) Ground Reaction Forces for a drop jump from 3m for different scenarios.(b) is a zoom in version of the region defined by the green dotted rectangle.

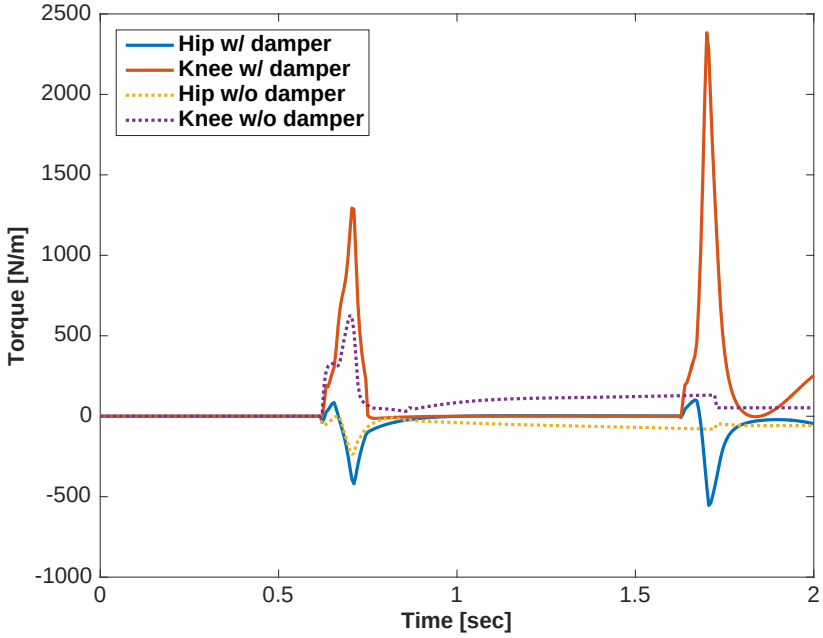

Figure 4.7: Joint torque output. With the damper torque generated are within the allowable bounds.

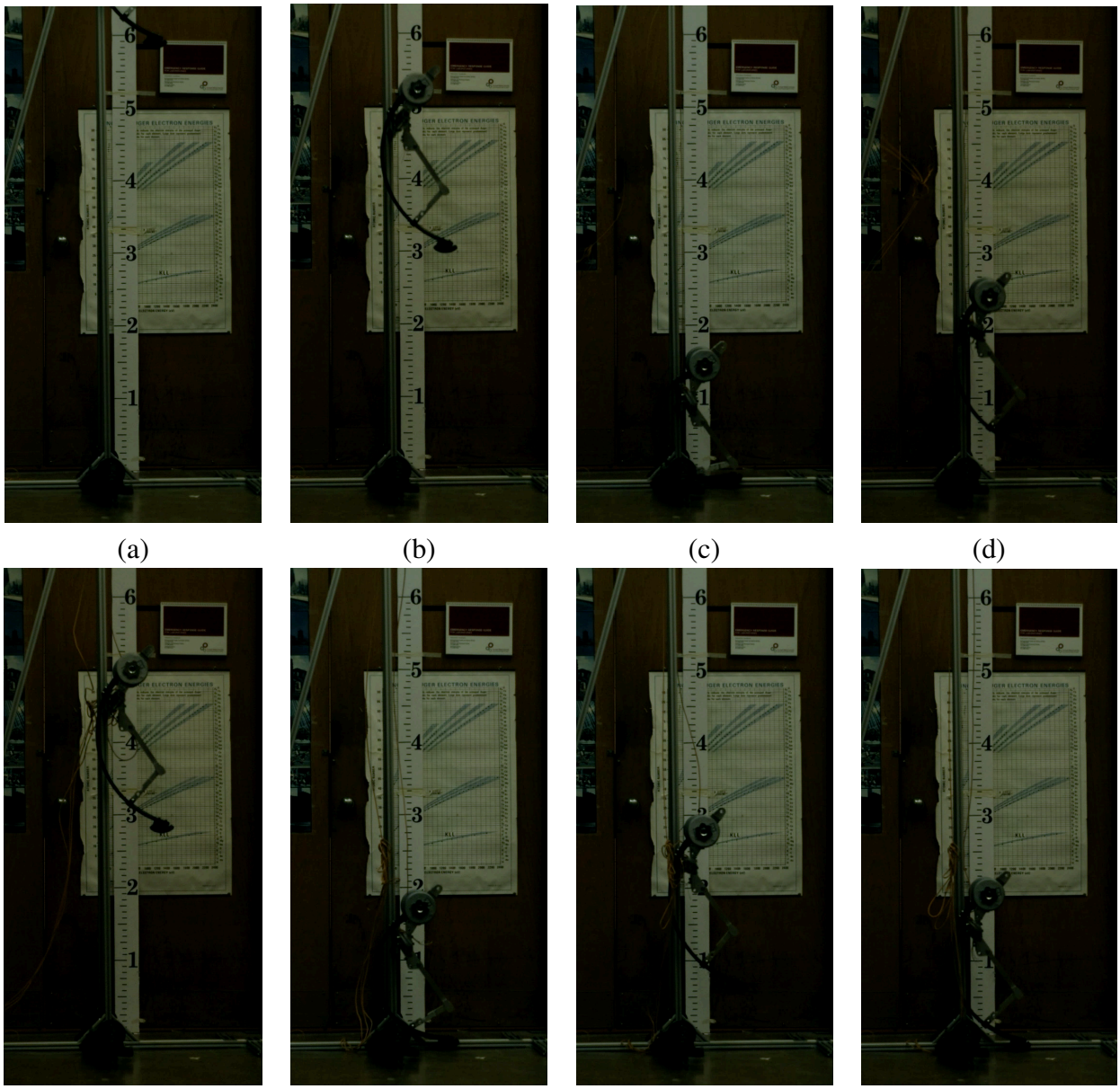

(a) (b) (c) (d)

(e) (f) (g) (h)

Figure 4.8: High speed video screenshot sequence of drop test set (1) from 6ft with 15kg payload mass. Leg bounced 3 times before coming to a rest with a max bounce height of 2ft 8in.

Figure 4.9: High speed video screenshot sequence of drop test set (2) from 6ft with 15kg payload mass. Leg bounced only once.

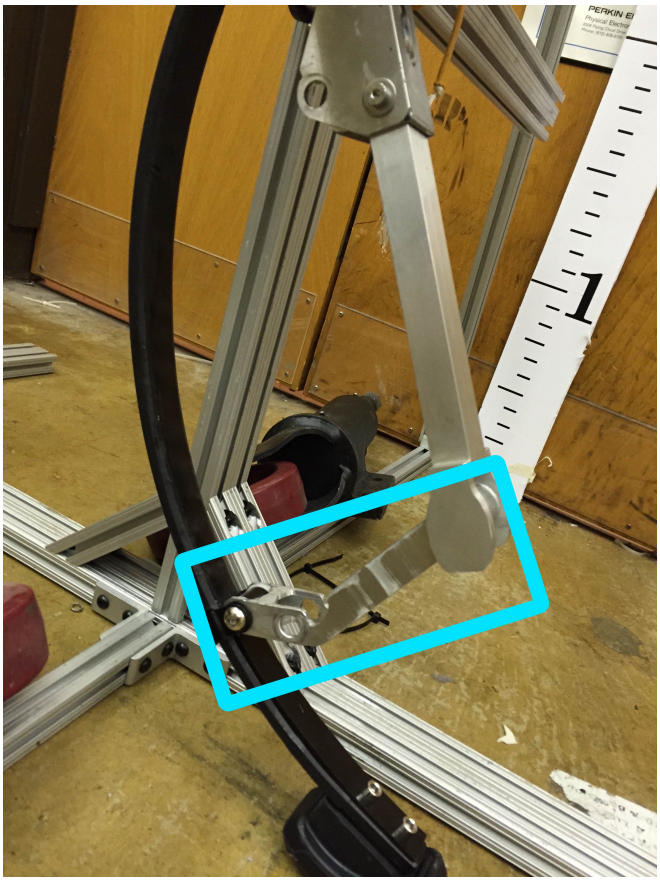

Figure 4.10: Image of bent shin component after a drop jump from 6ft with 30kg of payload with MR-damper set to its maximum value.

Chapter 5

Conclusion and Future Work

5.1 Summary

In this work we tackled the high level aim of extending bipedal robots' agility and capabilities by focusing on the specific task of safely drop jumping from a height of at least 3 meters. Inspired by active suspension systems in automobiles we proposed the mechanical design of a new leg for a bipedal system. The main impact attenuator component of the robot is the shin. A fiberglass leaf spring in parallel with a magneto-rheological damper make up the shin. Our design meets all the engineering specifications set in Section 2.2.

To validate our proposed design we developed a detailed model of the robotic leg with MATLAB's Simscape toolbox. We demonstrated through simulation the need of a physical damping element to be able to perform controllable drop jumps. Additionally, inspired by humans knee cushion strategy for landing we implemented an optimal impedance control. CMA-ES optimization algorithm was used to find the optimal controller gains for different drop heights. In simulation a maximum drop jumps of 6m without bouncing was achieved. For out target case of 3m our design and simple controller achieved a $5 \times 10^4 N$ reduction in the peak GRF.

With promising simulations results we built the shin section of the proposed leg design. To compare to simulation results we performed drop tests with and without the MR damper. We found that with the MR damper we managed to come to a rest after one bounce of only 5 inches. We also found that the MR damper's minimum damping coefficient value was too large for the size of the system. There was not sufficient load on the damper to notice the effect of different damping coefficients.

5.2 Future Work

There is still an extensive amount of work to be done with HIL leg. Following the organization of this thesis we divided the future work sections into two parts: (1) possible changes/improvements that could be done to the design of the robot, (2) future work in the controls algorithms and strategies. The following suggestions are planned to completed by the end of Summer 2016.

5.2.1 Mechanical Design

Promising simulation results of the HIL leg as well as satisfactory drop test with the bottom half of the leg have been shown. Therefore, a logical future step is to build a full version of the HIL leg. Having a complete prototype will allow us to deploy and test control algorithms to perform safe landings.

Some tasks like running require opposite requirements than drop landing. For example in running you want to minimize energy lost while in drop landing you want to maximize it. From the drop test we know that the MR damper has a large passive damping coefficient that is not desirable. A damping mechanism that can be completely turned-off so that there is no damping would be ideal. A potential method to achieve this is to add a clutch between the damper and the shin linkage. This will allow to actively engage and disengage the damper from the leg's mechanics.

Currently our primary source of protection for the robot leg is the spring in the shin. Additional passive elements such as; an outer shell, and/or foam/rubber padding can be added around the leg to protect it against impacts made not with the foot.

Sensing of the robot has a very important role on the controllability of the robot. Therefore, even small changes can have an important impact on its performance. Currently, the robot acceleration is estimated through the differentiation of the joint encoder position values. Adding a IMU will improve acceleration measurements. Additionally, strain gauges can be implemented to improve force measurements.

5.2.2 Controls

The HIL leg is an novel robotic platform and one of few human-adult size that have a semi-active damping element. This makes it a good platform to test new control strategies that take advantage of the damping element. HIL is intended to perform a wide range of dynamic maneuvers besides landing. Developing and implementing controls to walk, run and jump are interesting directions we would like to explore.

There has been significant advances in the realm of optimal control theory for systems with hybrid dynamics. Posa et al. [39] proposed an an optimal control algorithm to perform optimization through contact that will output optimal control inputs and contact sequences. This approach could be useful to determine optimal landing sequences that minimize impact forces.

5.3 Conclusion

The focus of this thesis work has been to present a mechanical robotic system that extents the current bipedal systems' walking and running capabilities to also perform the explosive motion of drop jumping. Through the implementation of simple optimal control strategies that take advantage of damping elements we showed that physical dampers are useful for legged systems.

The important message to take from this thesis is that a robot is a unified dynamic system comprised of electronics, software, and mechanical components. Therefore, significant thought has to be placed to what component(s) of a robot will aid to achieve a given task. For our specific

task of drop jumping, a physical semi-active damper is an important component. It maybe that for other explosive maneuvers such as running and jumping up it is not useful. Thus, increasing adaptability and not designing a robot for one unique task, is necessary if we want legged system to be deployable in the real world.

Further, there is still much work to be done in the field of legged and specifically bipedal robots. We intend to continue the work presented on this thesis. It is planned that by the end of summer 2016 we have a full working prototype of the proposed high impact landing robotic leg.

Part 2

Development of a Testbed for Nano Quadcopters

Chapter 6

Introduction

6.1 Motivation & Background

In recent years quadrotors have gained substantial popularity in both commercial and research environments. Commercially you can find a wide range of quadrotors ranging in size, cost, and capabilities designed for hobbyist entertainment, aerial photography, and surveillance to name few. In research its become a go-to platform for the study of under-actuated mechanical systems. Quadrotors are versatile systems capable supporting a wide range of payloads and performing very dynamic and agile maneuvers. Despite the advances thus far, there are still many interesting control problems to solve.

One area our research group is interested is the control of swarms of quadrotors. To be able to test advanced control algorithm a reliable and robust testbed is required. The nano quadcotper Crazyflie by Bitcraze [43] is a good platform for research. Its small form factor make it an ideal tool for research in swarms, path finding and failure recovery. The hardware and software are both open-source. This makes the platform flexible and easy to modify to implement our own control algorithms. Many control algorithms require precise 3D position measurements of the quad rotors. A common method to acquire this data is to fly the quadrotors in a motion capture arena. It is also common to have a base station to run the controller online but off-board. Therefore, a control framework is required that interfaces all these necessary components.

The aim of this work is to develop and implement a control framework for the Crazyflie Nano Quadrotor so it can be used as a test platform for different control algorithms developed by our research group. Due to the popularity of quadrotors in research you can find in the literature many different implementation of a control framework [44, 45]. However, they not all use the Crazyflie quadrotor. We implement a similar architecture to that proposed by Furci et al.[46], but use the control law proposed by Mellinger et al.[44].

6.2 Contribution

In this work we make the following contributions:

- Describe and implement a complete system architecture to test advance controls on the nano quadcopter Crazyflie. Control laws are implemented in MATLAB/Simulink and

commands are send via UDP to a python client that relays the commands to the Crazyflie via the USB dogle Crazyradio PA.

- Performed a system identification to determine the thrust profile of the Crazyflie relative to the input command.
- Developed a detail 3D CAD model of the Crazyflie model that was used to design a lightweight easy to manufacture frame that protects the Crazyflie propellers and provides room to mount the reflective markers.
- Validated the control architecture by means of experimentation. Implemented the position control proposed by Mellinger et al.[44] in MATLAB/Simulink an successfully showed hover and trajectory following.

Chapter 7

Hardware & Software

7.1 Crazyflie 2.0 Platform

The Crazyflie is a nano quadcopter designed and built by Bitcraze AB. The software and hardware are open source making it a convenient platform to develop on. Its small $18cm^2$ footprint and 27g mass make it ideal for flying indoors in a lab environment especially when you plan to have a swarm of quadcopters. We work with the second version of the Crazyflie released in December 2015 named Crazyflie 2.0.

7.1.1 Microcontroller

The Crazyflie 2.0 is architectured around 2 microcontrollers. The STM32F405, Cortex-M4@160MHz, runs the main firmware. It handles the onboard flight control,telemetry and all communication algorithms. Additionally, most the expansion port are connected to the STM32F405. The NRF51, Cortex-M0, handles radio communication and power management. It acts as a radio bridge between the raw communication data packages and the STM32F405.

7.1.2 On-Board sensors

The Crazyflie is equipped with a 6-axis IMU (MPU-9250), which contains a 3-axis gyroscope and a 3-axis accelerometer in a single chip. The IMU measurements are used for estimate estimation and are compared to measurements obtained by the off-boar motion capture system. Additionally, the Crazyflie also has an on-board high precision barometer sensor (LPS25H). Though, we do not use the barometer, it could be used to estimate the quadrotor altitude.

7.1.3 Power & Propulsion

Crazyflie 2.0 is powered by a small single cell Lithium-Polymer (LiPo) battery. It supplies 3.7V an has a capacity of 240mAh. The manufacture indicate that with full charge battery you will get 7 minutes of flight time. However, with the addition of the reflective markers and frame the flight time reduced to around 5 minutes.

The quadrotor is propelled by four brushed DC motors that weigh only 1.7g and each drive a fixed-pitch plastic 45mm plastic propeller. The motors are coreless which in theory provides faster acceleration. They can produce 12000rpm per volt, with a nominal voltage of 4.2V. From this we can compute the theoretical maximal thrust that is predicted by the k_F parameter we will describe later.

A drawkback point about the Crazyflie is the use if brush motors. Most quadrotors use brushless motors, which use an electronic circuit to accurately regulate their speed with respect to the input signal. Due to friction in brush motors they require higher motor speeds, requiring more torque and consequently drawing more power from the battery.

7.1.4 Motion Capture Marker Frame

The motion capture system described in Section 7.2.1 requires reflective markers to be able to track the position of the Crazyflie Quadcopters. However, because of the small size of the quadcopter the motion capture system was not able to distinguish between the markers when placed directly on the quadcopter because of their close proximity. Therefore we designed a custom frame to mount the reflective markers and also protect the blades in case of a collision. The frame can be 3D printed or laser-cut. We chose to 3D print the frame in FDM as it resulted in a lighter frame weighing only 1.2g compared to a laser-cut frame of plexiglas weighing 2.4g.

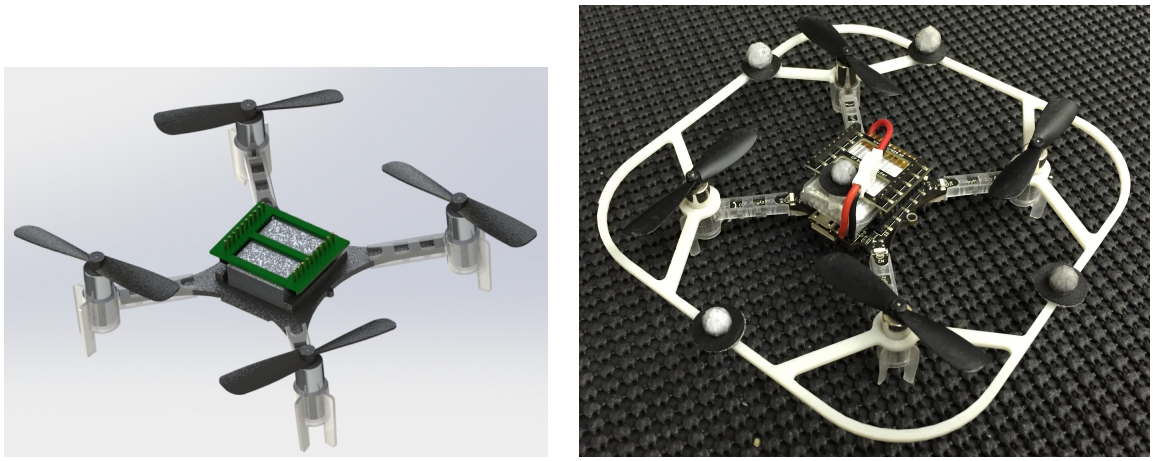

(a) (b)

Figure 7.1: (a) CAD rendering and (b) 3D printed frame used to protect quadcopter from collision and mount reflective markers

7.1.5 Communication Interface

Crazyflie 2.0 is equipped with Bluetooth LE as well as low-latency/long-range radio[43]. We chose to use the latter because of its ease and existing code to communicate with a PC. On the Crazyflie side radio communications are handled by a Nordic Semiconductor nRF51822 chip onboard while on the PC side by the Crazyradio PA. The Crazyradio PA is a 2.4 GhZ radio USB

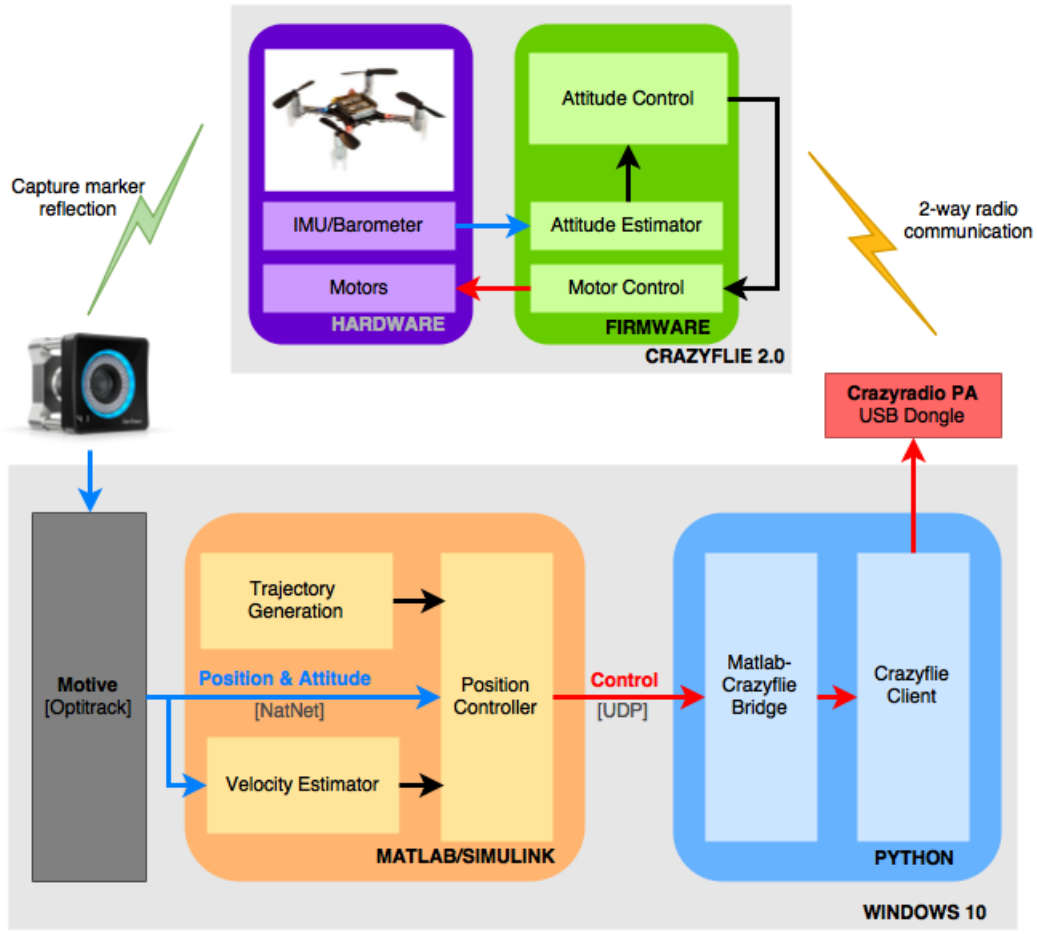

Figure 7.2: Schematic of system architecture

dongle based on nRF24LU1+ chip from Nordic Semiconductors. With the Crazyradio PA we can receive sensor data and send control commands from and to Crazyflie. The radios are rated to run at up to 2Mbps.

7.2 Control Architecture

The overall control architecture is depicted in Figure 7.2. The Crazyflie with reflective markers attached to it is operated in a confined fly arena that is surrounded by Optitrack motion capture cameras to measure the quadrotor's position. The raw camera data is streamed via ethernet to a base station that is running the Motive software. The processed data is streamed via the NatNet protocol to MATLAB/Simulink where the controller is implemented. The output of the controller is transmitted via UDP to the Python Crazyflie client that packs that data to be sent to the Crazyflia via the USB dongle Crazyradio PA. The control framework has been designed so that it can be easily replaced or modified.

7.2.1 Optical Motion Capture System

Our experimental setup contains an optical tracking system used to provide accurate measurements of the position of the quadrotor. Optical motion capture systems tracking have been widely used for similar experiments in the past. Our motion capture arena is composed of 12 Optritrack Prime 17W cameras. The infrared cameras localize the small reflecting markers we placed on the quadrotor. The system used in the experiment runs at 120Hz. The software Motives was used to process the data from the cameras and stream it to Matlab. The Optritrack and motive system provide both position and orientation measurements. We used a closed form linear system to estimate the velocity of Crazyflie.

7.2.2 MATLAB/Simulink Controller

MATLAB/Simulink programming environment is used to process data received from both the motion capture system Optitrack and Crazyflie. A custom 2nd-Level S-function block was developed using the Optitrack SDK to stream data into Simulink. Motion capture position data is numerically differentiated to calculate the Crazyflie's linear velocity. A position controller is implemented that outputs commands to the Crazyflie so that it will follow a user-defined trajectory. The commands are send via UDP to the Python client. "Stream Input" and "Stream Output" Simulink blocks are used to receive and send data between Simulink and the Ptyhon Client. More details on the controller implemented are described in Section 8.

7.2.3 Python Bridge and Client

The manufactures provide an open-source client application that make it easy to use different input devices (e.g. PlayStation 3 joystick, ZMQ) to teleoperate the Crazyflie. The client application has a user-friendly GUI that makes it easy to track the status of the Crazyflie. In addition to the client application provided by Bitcraze, an open-source Python API is available. The API makes it easy to interact with the USB Crazyradio to sent and receive data from one or multiple Crazyflies. The API was used to create a communication bridge between MATLAB/Simulink and the Crazyflie. The bridge makes it possible to send control commands (roll, pitch, yaw, and thrust) to quadrotor. Also, it is capable of receiving telemetry (IMU and barometer readings) from the Crazyflie and forward them to MATLAB/Simulink.

7.2.4 On-board Firmware

The Crazyflie Nano Quadcopter firmware is based on FreeRTOS, an open source realtime operating system. Commands are sent via the Crazyradio PA to the quadrotor using the Crazy RealTime Protocol (CRTP). The main firmware on the STM32F405 micro-controller runs all the communication, power, and sensors reading algorithms. In addition it implements an internal proportional integral derivative (PID) attitude controller that stabilizes the desired Euler angles commanded.

Chapter 8

Model & Control

8.1 Dynamical Model

The position of the quadrotor is defined with respect to an inertial frame $\{I\}$ as shown in Figure 8.1. The inertial frame is defined by axes x_I, y_I, and z_I with z_I pointing upwards. A body fixed frame $\{B\}$ is attached to the quadrotor's center of mass. We fly the quadrotor in "X" formation thus the axis x_B that coincides with the preferred forward direction is $45°$ CCW form the diagonal formed by motors M2 and M4. The z_B axis is perpendicular to plane of the rotors. A Z-X-Y Euler angles are used to model the rotation of the quadrotor with respect to the inertia frame. We define the Euler angles as follow:

Axis	Name	Symbol
Z	Yaw	ψ
X	Roll	ϕ
Y	Pitch	θ

and rotation matrix to transform from $\{B\}$ to $\{I\}$ is

$$R = \begin{bmatrix} c\psi c\theta - s\phi s\psi s\theta & -c\phi s\psi & c\psi s\theta + c\theta s\phi s\psi \\ c\theta s\psi + c\psi s\phi s\theta & c\phi c\psi & s\psi s\theta - c\psi c\theta s\phi \\ -c\phi s\theta & s\phi & c\phi c\theta \end{bmatrix} \tag{8.1}$$

where $c\phi$ and $s\phi$ denotes $\cos\phi$ and $\sin\phi$ respectively, and similar for θ and ψ. The position of the quadrotor with respected to the inertial frame is denoted by $\mathbf{r}$.

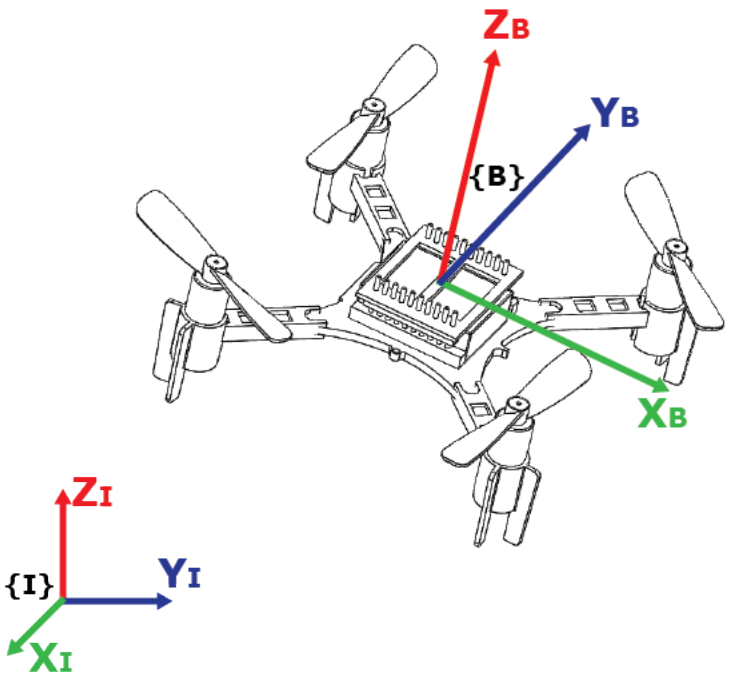

Figure 8.1: Sketch of coordinate system used. Note convention of positive Z_B axis pointing up.

The equations of motion of the system are derived from Newton's second law. Two forces act on the system; 1) gravity in the $-z_I$ direction and 2) thrust forces F_i generated by each propeller in the $+z_B$ direction. We represent the equation of motion in the inertial frame:

$$m\ddot{\mathbf{r}} = \begin{bmatrix} 0 \\ 0 \\ -mg \end{bmatrix} + R \begin{bmatrix} 0 \\ 0 \\ \sum F_i \end{bmatrix} \qquad \text{for } i = 1, 2, 3, 4 \tag{8.2}$$

where m is the mass of the quadrotor, and $g = 9.81 m/s^2$ the acceleration due to gravity.

8.2 Motor Model

The vertical force produced by each combination of motor and propeller is modeled according to

$$F_i = k_F w_i^2 \qquad \text{for } i = 1, 2, 3, 4 \tag{8.3}$$

where w_i represent the angular speed of each propeller $i \in \{1, 2, 3, 4\}$ and F_i the vertical force they each. The parameter k_F was estimated using two methods for redundancy. Method 1) we know that when the quadrotor is in perfect hover $mg = 4k_F w_h^2$, where w_h is the propeller speed at hover. Since we know mg, and a w_h from experiments, we can compute k_F. Method 2) We place the quadrotor upside-down on a scale, command angular velocities and record the thrust generated. Using a linear interpolation we can extract the value of k_F. The value of k_F is important for the control law implemented.

8.3 Position Control

In this section we briefly describe the implemented control law proposed by Mellinger et al.[44] that reaches the desired position and yaw angle with zero linear and angular velocities. The control input are desired roll ϕ^{des} and pitch θ^{des} angles, yaw rate Δw_ψ and Δw_F thrust. The trajectory and yaw we want to track are represent by $r_T(t)$ and $\psi_T(t)$ respectively. The command accelerations, $\ddot{r}_i^{des}$, are calculated from PID feedback of the position error, $e_i = (r_{i,T} - r_i)$, as

$$(\ddot{r}_{i,T} - \ddot{r}_i^{des}) + k_{d,i}(\dot{r}_{i,T} - \dot{r}_i) + k_{p,i}(r_{i,T} - r_i + k_{i,i}) \int (r_{i,T} - r_i) = 0 \tag{8.4}$$

where $\dot{r}_{i,T} = \dot{r}_{i,T} = 0$ for hover. Equation (8.2) is linearized to get the relationship between the desired accelerations and roll and pitch angles

$$\ddot{r}_1^{des} = g(\theta^{des} \cos\psi_T + \phi^{des} \sin\psi_T) \tag{8.5}$$

$$\ddot{r}_2^{des} = g(\theta^{des} \sin\psi_T + \phi^{des} \cos\psi_T) \tag{8.6}$$

$$\ddot{r}_3^{des} = \frac{8k_f w_h}{m} \Delta w_F \tag{8.7}$$

These relationships are inverted to compute the desired roll and pitch angles as well as Δw_F from the desired accelerations. Δw_ψ is calculated from simple PD feedback the yaw error

$$\phi^{des} = \frac{1}{g}(\ddot{r}_1^{des} \sin\psi_T - \ddot{r}_2^{des} \cos\psi_T) \tag{8.8}$$

$$\theta^{des} = \frac{1}{g}(\ddot{r}_1^{des} \cos\psi_T - \ddot{r}_2^{des} \sin\psi_T) \tag{8.9}$$

$$\Delta w_F = \frac{m}{8k_F w_h} \ddot{r}_3^{des} \tag{8.10}$$

$$\Delta w_\psi = k_{p,\psi}(\psi_T - \psi) + k_{d,\psi}(\dot{\psi}_T - \dot{\psi}) \tag{8.11}$$

Chapter 9

Experiments & Results

To validate the proposed overall system architecture and control, in this section we present results of three experiments conducted. All test start with a Crazyflie with motors off sitting about 1m above the ground on a box. A launch sequence is executed before the position control takes command.

9.1 Altitude Hold

In the first test the quadrotor motion is constrained to only the vertical direction. We confine the movement of the Crazyflie by fixing it to a PVC structure with two wires running vertically that guide the motion of the Crazyflie (see Figure 9.1). The test setup decouples the roll, pitch, and yaw degrees of freedom. Thus, it is easier to find reasonable gains for the PID altitude control law portion of the position control.

Figure 9.1: PVC rig used to constrain the motion of Crazyflie to just vertical

The controller successfully lunch the quadcopter from its base and controlled it to track the desired altitude value. The results are shown in Figure 9.2. The initial overshoot is due to

the launch sequence, and this can be easily improved. Reducing the 20 second settling time is desirable but not necessary. We found that reducing the settling time diminished the tracking performance.

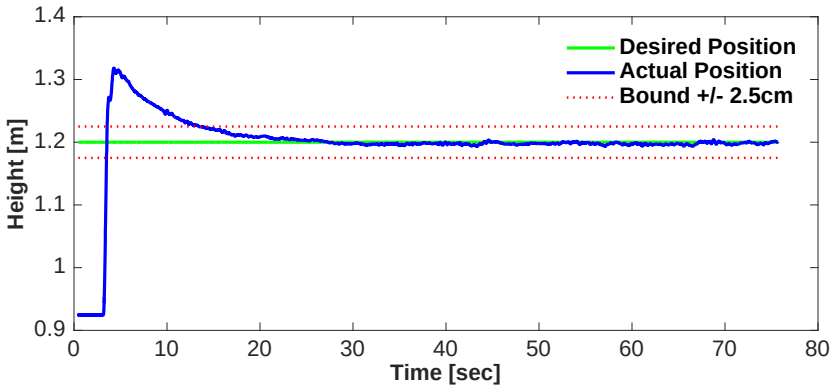

Figure 9.2: Altitude hold test results, desired (green solid) and actual (blue solid) height position of Crazyflie. The initial overshoot is due to the takeoff sequence.

9.2 Hover Control

Working on top of the results from the altitude hold test we remove the PVC structure. With the Crazylie free to move in any direction limited only by its own dynamics we tested the capability to maintain a hover position defined by an (x,y,z) coordinate point. Figure 9.3 show the position measurements from the motion capture system when trying to maintain a stable hover at (X,Y,Z). The control commands generated by the implemented control law are shown in Figure 9.4. A steady hover was achieved. In the x-direction position was within 6cm while in the y-direction within 10cm.

9.3 Trajectory Following

The final evaluation of the controller was trajectory following. The reference trajectory to follow was a circular path counterclockwise of radius $1m$ with a period time of $15sec.$. None of the controller gains where retuned for this specific task. The gains obtained from the hover experiment where used. Figure 9.5 depicts the comparison between the desired and the actual X-Y trajectory the quadcopter took. The controller managed to take-off and moved into position to track the trajectory. However, the controller is not perfect. The feedforward command was modified to improve the performance. The best we obtained was to track the trajectory within 6cm in the x-direction and 15cm in the y-direction.

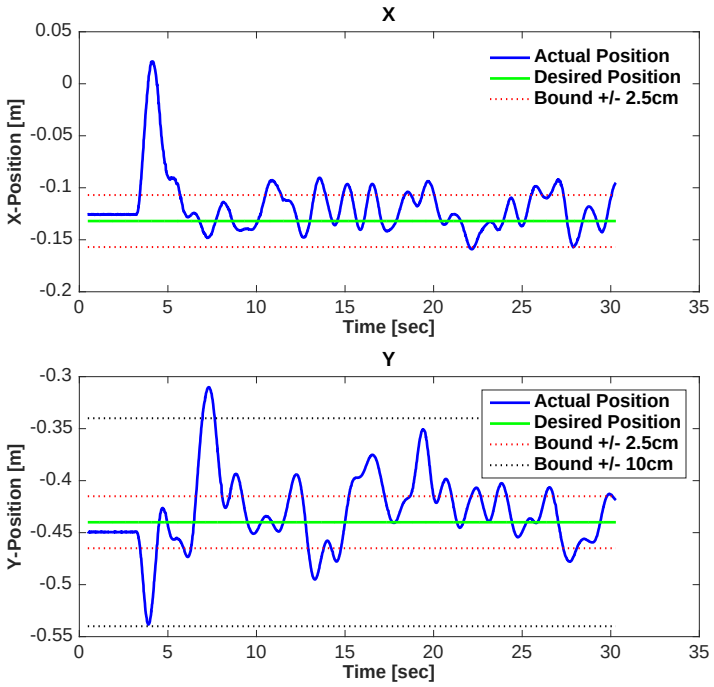

Figure 9.3: Recorded X and Y position of Crazyflie while trying to hover in place. There are oscillations are within 10cm

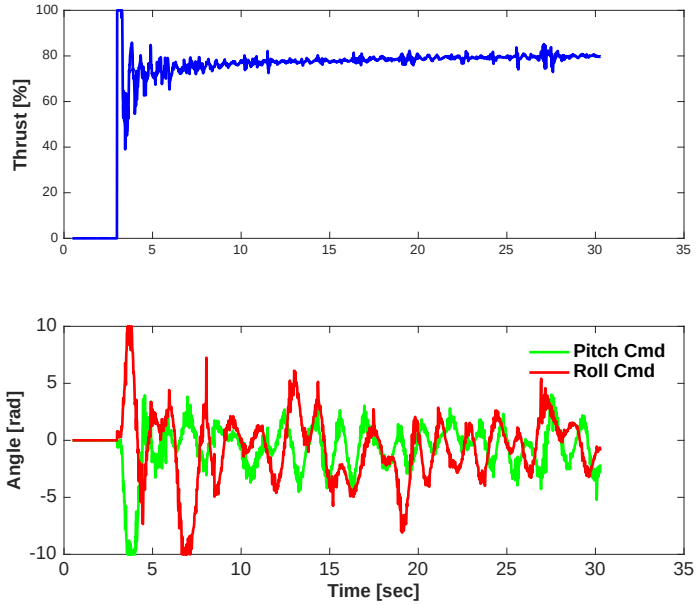

Figure 9.4: Thrust, roll, and pitch commands to maintain a steady hover.

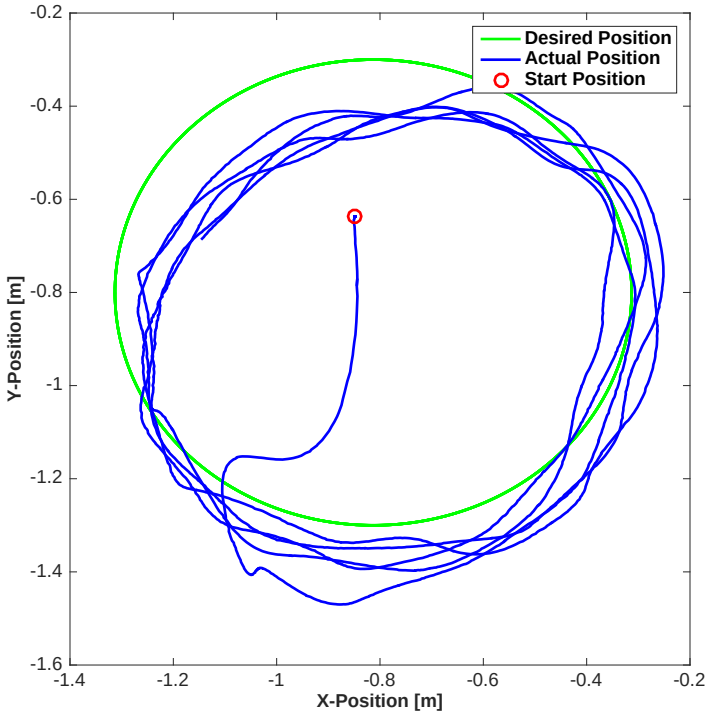

Figure 9.5: X-Y plot of Crazyflie following a circular trajectory counterclockwise. Trajectory following is not perfect in addition to the oscillations in the x-y position there is an offset of 15cm in the y direction.

Chapter 10

Conclusion and Future Work

10.1 Conclusion

In this work we have presented and implemented a nano aerial vehicle testbed for advance control algorithms. Through experiments we have shown a working control framework that manages to stabilize the position of the nano quadcopter Crazyflie inside a motion capture arena. We implemented the control proposed by Mellinger et al.[44]. We also showed the ability follow a reference trajectory within 15cm.

For the type of demanding applications our research group is interested in, a higher tracking tolerance is required. We want to reduce the 15cm error to be between 2-3cm. Having established and implemented the testbed architecture it simplifies the process of tuning gains and/or modifying the position control to improve performance.

10.2 Future Work

There are still some improvements that can be made to the control architecture to be more user-friendly. At the moment it is required to initialize and run the MATLAB/Simulink and Python scripts separately. It would be better to include a block in Simulink that will automatically run the Python script. Also, though possible the current code does not allow for easily allow to control multiple Crazyflies. A more user-friendly front end GUI will be developed to ease the addition of connecting multiple Crazyflies.

Though the performance of the current control law is satisfactory this can be significantly improved. Implementing a LQR controller could improve the performance. Additionally, the onboard attitude control gains have not been modified from those set by the manufacturer. Retuning these gains may improve performance.

A native C++ based S-Function Crazyflie library was developed that would perform all the same functions that the Python API does. The native Simulink Crazyflie library would simplify the control architecture by removing all the python components. However, at the moment the code is very inefficient and is introducing significant delays to the control loop that make it impossible to fly the quadrotors.

References

[1] S. Seok, A. Wang, M. Y. Chuah, D. Otten, J. Lang, and S. Kim, "Design principles for highly efficient quadrupeds and implementation on the mit cheetah robot," in *Robotics and Automation (ICRA), 2013 IEEE International Conference on*. IEEE, 2013, pp. 3307–3312. (document), 1.2, 2.3

[2] K. Fujiwara, F. Kanehiro, S. Kajita, K. Yokoi, H. Saito, K. Harada, K. Kaneko, and H. Hirukawa, "The first human-size humanoid that can fall over safely and stand-up again," in *IEEE-RSJ International Conference on Intelligent Robots and Systems, Las Vegas, NV, USA*, vol. 27, 2003, pp. 1920–1926. (document), 1.2.2, 1.2

[3] S.-H. Lee and A. Goswami, "Fall on backpack: Damage minimizing humanoid fall on targeted body segment using momentum control," in *ASME 2011 International Design Engineering Technical Conferences and Computers and Information in Engineering Conference*. American Society of Mechanical Engineers, 2011, pp. 703–712. (document), 1.2.2, 1.2

[4] Y. Ito, T. Nakaoka, J. Urata, Y. Nakanishi, K. Okada, and M. Inaba, "Design and development of a tendon-driven and axial-driven hybrid humanoid leg with high-power motor driving system," in *Humanoid Robots (Humanoids), 2012 12th IEEE-RAS International Conference on*. IEEE, 2012, pp. 475–480. (document), 1.2.3, 1.3

[5] J. A. Grimes and J. W. Hurst, "The design of atrias 1.0 a unique monopod, hopping robot," in *Proceedings of the 2012 International Conference on Climbing and Walking Robots and the Support Technologies for Mobile Machines*, 2012, pp. 548–554. (document), 1.2.3, 1.3, 2.3

[6] M. Hutter, C. D. Remy, M. A. Hoepflinger, and R. Siegwart, "Scarleth: Design and control of a planar running robot," in *Intelligent Robots and Systems (IROS), 2011 IEEE/RSJ International Conference on*. IEEE, 2011, pp. 562–567. (document), 1.2.3, 1.3, 2.3

[7] D. Truong and K. Ahn, *MR fluid damper and its application to force sensorless damping control system*. INTECH Open Access Publisher, 2012. (document), 2.5.1, 2.4, 3.1

[8] P. J. McNair, H. Prapavessis, and K. Callender, "Decreasing landing forces: effect of instruction," *British Journal of Sports Medicine*, vol. 34, no. 4, pp. 293–296, 2000. 1.1

[9] H. Makaruk and T. Sacewicz, "The effect of drop height and body mass on drop jump intensity," *Biology of Sport*, vol. 28, no. 1, p. 63, 2011. 1.1, 1.2.1

[10] A. Lees, "Methods of impact absorption when landing from a jump," *Engineering in Medicine*, vol. 10, no. 4, pp. 207–211, 1981. 1.2.1

[11] M. A. Lafortune, E. M. Hennig, and M. J. Lake, "Dominant role of interface over knee angle for cushioning impact loading and regulating initial leg stiffness," *Journal of biomechanics*, vol. 29, no. 12, pp. 1523–1529, 1996. 1.2.1

[12] P. DeVita and W. A. Skelly, "Effect of landing stiffness on joint kinetics and energetics in the lower extremity," *Med Sci Sports Exerc*, vol. 24, no. 1, pp. 108–115, 1992. 1.2.1

[13] S.-N. Zhang, B. T. Bates, and J. S. Dufek, "Contributions of lower extremity joints to energy dissipation during landings." *Medicine and Science in Sports and Exercise*, vol. 32, no. 4, pp. 812–819, 2000. 1.2.1

[14] J. T. Weinhandl, J. D. Smith, and E. L. Dugan, "The effects of repetitive drop jumps on impact phase joint kinematics and kinetics," *Journal of applied biomechanics*, 2011. 1.2.1

[15] R. J. Standing and P. S. Maulder, "A comparison of the habitual landing strategies from differing drop heights of parkour practitioners (traceurs) and recreationally trained individuals," *Journal of sports science & medicine*, vol. 14, no. 4, p. 723, 2015. 1.2.1

[16] K. Fujiwara, F. Kanehiro, S. Kajita, and H. Hirukawa, "Safe knee landing of a human-size humanoid robot while falling forward," in *Intelligent Robots and Systems, 2004.(IROS 2004). Proceedings. 2004 IEEE/RSJ International Conference on*, vol. 1. IEEE, 2004, pp. 503–508. 1.2.2

[17] K. Fujiwara, F. Kanehiro, S. Kajita, K. Kaneko, K. Yokoi, and H. Hirukawa, "Ukemi: falling motion control to minimize damage to biped humanoid robot." in *IROS*, 2002, pp. 2521–2526. 1.2.2

[18] K. Fujiwara, S. Kajita, K. Harada, K. Kaneko, M. Morisawa, F. Kanehiro, S. Nakaoka, and H. Hirukawa, "An optimal planning of falling motions of a humanoid robot," in *Intelligent Robots and Systems, 2007. IROS 2007. IEEE/RSJ International Conference on*. IEEE, 2007, pp. 456–462. 1.2.2, 3.3

[19] J. Wang, E. C. Whitman, and M. Stilman, "Whole-body trajectory optimization for humanoid falling," in *American Control Conference (ACC), 2012*. IEEE, 2012, pp. 4837–4842. 1.2.2

[20] K. Ogata, K. Terada, and Y. Kuniyoshi, "Falling motion control for humanoid robots while walking," in *Humanoid Robots, 2007 7th IEEE-RAS International Conference on*. IEEE, 2007, pp. 306–311. 1.2.2

[21] S.-k. Yun, A. Goswami, and Y. Sakagami, "Safe fall: Humanoid robot fall direction change through intelligent stepping and inertia shaping," in *Robotics and Automation, 2009. ICRA'09. IEEE International Conference on*. IEEE, 2009, pp. 781–787. 1.2.2

[22] H. Dallali, P. Kormushev, N. G. Tsagarakis, and D. G. Caldwell, "Can active impedance protect robots from landing impact?" in *Humanoid Robots (Humanoids), 2014 14th IEEE-RAS International Conference on*. IEEE, 2014, pp. 1022–1027. 1.2.3

[23] G. A. Pratt and M. M. Williamson, "Series elastic actuators," in *Intelligent Robots and Systems 95.'Human Robot Interaction and Cooperative Robots', Proceedings. 1995 IEEE/RSJ International Conference on*, vol. 1. IEEE, 1995, pp. 399–406. 1.2.3

[24] K. Radkhah and O. von Stryk, "A study of the passive rebound behavior of bipedal robots

with stiff and different types of elastic actuation," in *Robotics and Automation (ICRA), 2014 IEEE International Conference on*. IEEE, 2014, pp. 5095–5102. 1.2.3

[25] R. Niiyama and Y. Kuniyoshi, "Design of a musculoskeletal athlete robot: A biomechanical approach," in *Proc. 12th Int. Conf. on Climbing and Walking Robots and the Support Technologies for Mobile Machines*, 2009, pp. 173–180. 1.2.3

[26] A. Ananthanarayanan, M. Azadi, and S. Kim, "Towards a bio-inspired leg design for high-speed running," *Bioinspiration & biomimetics*, vol. 7, no. 4, p. 046005, 2012. 1.2.3

[27] J. P. Schmiedeler and K. J. Waldron, "Impact analysis as a design tool for the legs of mobile robots," in *Advances in Robot Kinematics*. Springer, 2000, pp. 129–136. 2.3

[28] A. Böck, "Device for helping a person to walk," Apr. 13 2004, uS Patent 6,719,671. [Online]. Available: http://www.google.com/patents/US6719671 2.5

[29] H. Brown, I. Nourbakhsh, and G. Zeglin, "Energy storage device used in locomotion machine," May 6 2003, uS Patent 6,558,297. [Online]. Available: http://www.google.com/patents/US6558297 2.5

[30] H. L. Xie, F. Li, F. Wang, and Y. X. Liu, "Intelligent control of brhl based on mr damper," in *Applied Mechanics and Materials*, vol. 10. Trans Tech Publ, 2008, pp. 466–470. 2.5

[31] J. Chen and W. Liao, "Design, testing and control of a magnetorheological actuator for assistive knee braces," *Smart Materials and Structures*, vol. 19, no. 3, p. 035029, 2010. 2.5

[32] MATLAB, *version 8.3.0 (R2015b)*. Natick, Massachusetts: The MathWorks Inc., 2015. 3.1, 3.3

[33] W. J. Palm, *System dynamics*. McGraw-Hill, 2010. 3.1

[34] K. Hunt and F. Crossley, "Coefficient of restitution interpreted as damping in vibroimpact," *Journal of applied mechanics*, vol. 42, no. 2, pp. 440–445, 1975. 3.2

[35] E. R. Westervelt, J. W. Grizzle, C. Chevallereau, J. H. Choi, and B. Morris, *Feedback control of dynamic bipedal robot locomotion*. CRC press, 2007, vol. 28. 3.3

[36] P. E. Gill, W. Murray, and M. A. Saunders, "SNOPT: An SQP algorithm for large-scale constrained optimization," *SIAM Rev.*, vol. 47, pp. 99–131, 2005. 3.3

[37] G. Schultz and K. Mombaur, "Modeling and optimal control of human-like running," *Mechatronics, IEEE/ASME Transactions on*, vol. 15, no. 5, pp. 783–792, 2010. 3.3

[38] K. Fujiwara, S. Kajita, K. Harada, K. Kaneko, M. Morisawa, F. Kanehiro, S. Nakaoka, and H. Hirukawa, "Towards an optimal falling motion for a humanoid robot," in *Humanoid Robots, 2006 6th IEEE-RAS International Conference on*. IEEE, 2006, pp. 524–529. 3.3

[39] M. Posa, C. Cantu, and R. Tedrake, "A direct method for trajectory optimization of rigid bodies through contact," *The International Journal of Robotics Research*, vol. 33, no. 1, pp. 69–81, 2014. 3.3, 5.2.2

[40] C. Igel, T. Suttorp, and N. Hansen, "A computational efficient covariance matrix update and a (1+1)-CMA for evolution strategies," in *Proceedings of the 8th annual conference on genetic and evolutionary computation GECCO*. ACM, 2006, pp. 453–460. 3.3

[41] N. Shafii, N. Lau, and L. P. Reis, "Learning a fast walk based on zmp control and hip

height movement," in *Autonomous Robot Systems and Competitions (ICARSC), 2014 IEEE International Conference on*. IEEE, 2014, pp. 181–186. 3.3

[42] G. Capi, Y. Nasu, L. Barolli, K. Mitobe, and K. Takeda, "Application of genetic algorithms for biped robot gait synthesis optimization during walking and going up-stairs," *Advanced robotics*, vol. 15, no. 6, pp. 675–694, 2001. 3.3

[43] B. io. (2016) Bitcraze io crazyflie 2.0. [Online]. Available: https://www.bitcraze.io/crazyflie-2/ 6.1, 7.1.5

[44] D. Mellinger, N. Michael, and V. Kumar, "Trajectory generation and control for precise aggressive maneuvers with quadrotors," *The International Journal of Robotics Research*, p. 0278364911434236, 2012. 6.1, 6.2, 8.3, 10.1

[45] B. Landry *et al.*, "Planning and control for quadrotor flight through cluttered environments," Ph.D. dissertation, Massachusetts Institute of Technology, 2015. 6.1

[46] M. Furci, G. Casadei, R. Naldi, R. Sanfelice, and L. Marconi, "An open-source architecture for control and coordination of a swarm of micro-quadrotors," in *Unmanned Aircraft Systems (ICUAS), 2015 International Conference on*. IEEE, 2015, pp. 139–146. 6.1